

# Transformer Transforms Salient Object Detection and Camouflaged Object Detection

Yuxin Mao<sup>†</sup>, Jing Zhang<sup>‡</sup>, Zhexiong Wan, Yuchao Dai\*,  
Aixuan Li, Yunqiu Lv, Xinyu Tian, Deng-Ping Fan and Nick Barnes

**Abstract**—The transformer networks, which originate from machine translation, are particularly good at modeling long-range dependencies within a long sequence. Currently, the transformer networks are making revolutionary progress in various vision tasks ranging from high-level classification tasks to low-level dense prediction tasks. In this paper, we conduct research on applying the transformer networks for salient object detection (SOD). Specifically, we adopt the dense transformer backbone for fully supervised RGB image based SOD, RGB-D image pair based SOD, and weakly supervised SOD via scribble supervision. As an extension, we also apply our fully supervised model to the task of camouflaged object detection (COD) for camouflaged object segmentation. For the fully supervised models, we define the dense transformer backbone as feature encoder, and design a very simple decoder to produce a one channel saliency map (or camouflage map for the COD task). For the weakly supervised model, as there exists no structure information in the scribble annotation, we first adopt the recent proposed Gated-CRF loss to effectively model the pair-wise relationships for accurate model prediction. Then, we introduce self-supervised learning strategy to push the model to produce scale-invariant predictions, which is proven effective for weakly supervised models and models trained on small training datasets. Extensive experimental results on various SOD and COD tasks (fully supervised RGB image based SOD, fully supervised RGB-D image pair based SOD, weakly supervised SOD via scribble supervision, and fully supervised RGB image based COD) illustrate that transformer networks can transform salient object detection and camouflaged object detection, leading to new benchmarks for each related task.

**Index Terms**—Vision Transformer, Salient Object Detection, Camouflaged Object Detection.

## 1 INTRODUCTION

Visual salient object detection [1, 2, 3, 4, 5, 6, 7] aims to localize the regions of an image that attract human attention. For static image based salient object detection, researchers mostly consider one of two fully supervised tasks, namely RGB image based salient object detection [1, 2] and RGB-D image pair based salient object detection [3, 4]. To reduce the labeling effort, several weakly supervised salient object detection models have been proposed to learn saliency with image-level supervision [6], scribble supervision [5] or learn saliency directly from noisy labeling [8, 9].

Before the deep learning revolution, conventional salient object detection models [10, 11] used handcrafted features as shown in Fig. 2, which define saliency as contrast [12] between each pixel (or superpixel) and the other pixels (or superpixels). In this way, the receptive field of the conventional handcrafted-feature based models is the entire image, which is global context as shown in Fig. 1, where saliency of the pixel colored in yellow depends on all the other pixels. However, the less representative handcrafted-feature limited their performance. The deep convolutional neural network (CNN) based salient object detection models [1, 2, 13, 14] achieve significant performance improvement

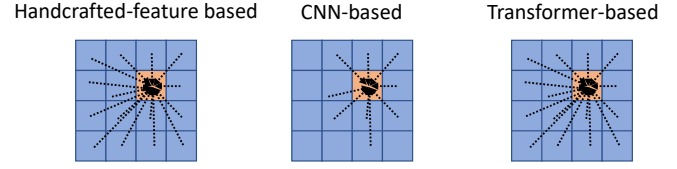


Fig. 1. Receptive field comparison of conventional handcrafted-feature based salient object detection models, CNN-based models and Transformer-based models.

compared with those handcrafted-feature based techniques with more sophisticated features extracted from the deep network.

The conventional deep CNN based SOD network usually includes two main parts: an encoder to extract different levels of features, and a decoder to aggregate features from different levels of the network for finer prediction. The encoder part is adopted from the trained backbone network on ImageNet, *e.g.*, VGG16 [15], ResNet50 [16], and the most effort for SOD models has been put on designing an effective decoder for feature aggregation [1, 2, 17]. The convolution operation can be efficiently parallelized using GPUs, and it can provide suitable inductive biases when extracting features from an image. However, two main issues exist in existing CNN based models. Firstly, due to weight sharing, the features extracted from the convolutional layer are translation invariant, and they are not sensitive to the global position of the feature. Secondly, the features extracted from the convolution layer are locally sensitive, and each operation only considers the local area of the image.

Usually, convolutional backbones have gradually larger receptive fields with the deeper layers, where the deepest level of

• Yuxin Mao, Zhexiong Wan, Yuchao Dai, Aixuan Li, Yunqiu Lv and Xinyu Tian are with School of Electronics and Information, Northwestern Polytechnical University, China.  
 • Jing Zhang and Nick Barnes are with School of Computing, Australian National University.  
 • Deng-Ping Fan is with the CS, Nankai University, Tianjin, China.  
 • <sup>†‡</sup>: Equal contributions.  
 • Corresponding author: Yuchao Dai (Email: daiyuchao@nwpu.edu.cn).

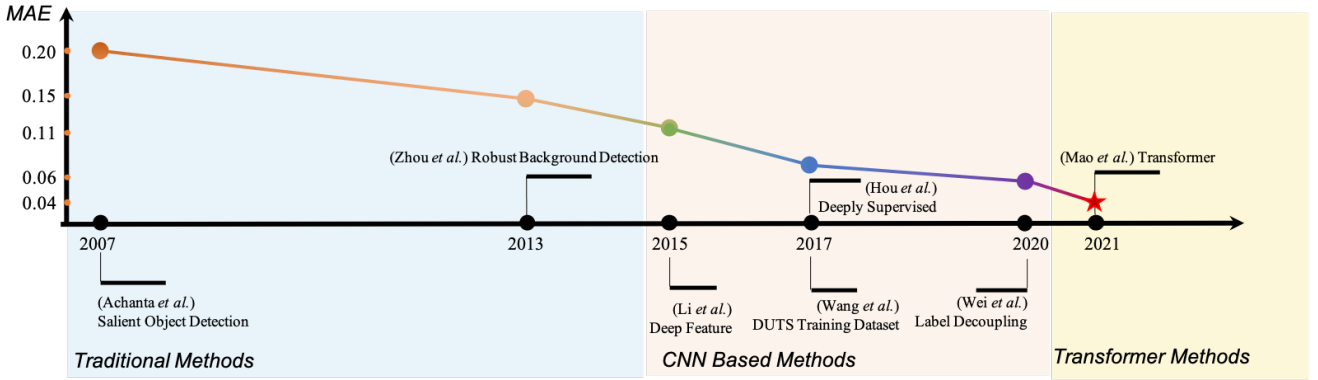


Fig. 2. A simplified timeline of salient object detection models, where the y-axis shows the mean absolute error (MAE) of related models on the DUT testing dataset [11]. Initially, Itti *et al.* [18] defined saliency detection as fixation prediction to predict the fixation points of salient objects. Then, Achanta *et al.* [19] introduced saliency detection as binary segmentation task to produce a segmentation map instead of a fixation map. The first CNN based deep saliency model [20] appeared in 2015, which replaced the handcrafted features with deep features. We introduce transformer backbone based salient object detection model with significantly improved model performance.

network has the largest receptive field. The main issue with these backbone networks is that the larger receptive field is obtained with the loss of structure information as a sacrifice. This is the reason for incorporating an additional decoder, which is used to recover the lost structure information by aggregating higher and lower level features. However, once the information is lost, it will not be fully recovered. Further, in theory, the receptive field of a CNN should cover the entire image, but many studies have shown that the actual receptive field of CNN is much smaller than the theoretical receptive field as shown in Fig. 1. In this way, a network with a larger receptive field without losing fine-grained information can be beneficial, especially for context based tasks, *e.g.*, SOD and COD, to achieve global context modeling.

Based on the limitations of convolutional neural networks described above, researchers found that the “Transformer” [21] has great potential to solve the limited receptive field issue in vision tasks. The advantage of the “Transformer” lies in the use of self-attention to capture global contextual information to establish a long-range dependency as shown in Fig. 1, and it can extract more meaningful features. Different from convolutional neural networks that focus on a small patch of the image with a sliding window wise convolution operation, the transformer network [21] performs global context modeling. Inspired by [22], we introduce the transformer backbone network to salient object detection to achieve a global receptive field at every stage of the encoder network. To test how the transformer backbone network contributes to SOD, we perform both fully supervised and weakly supervised learning to achieve salient object detection for both RGB image based and RGB-D image pair based SOD, leading to three new benchmark models. For the fully supervised models, we observe that the transformer backbone [22] has already encoded enough structure information at every stage of the network, we then design a very simple decoder to obtain a one-channel saliency map in the end. For the weakly supervised SOD setting, we adopt Gated-CRF loss [23] to recover the missing structure information in the weak annotation, and a self-supervised learning strategy to achieve effective model learning with a limited training dataset. As another binary segmentation task, we also extend our transformer based fully supervised learning framework to COD.

Our main contributions can then be summarized as: 1) we introduce the transformer backbone [22] to SOD and COD tasks

and achieve a new benchmark for fully supervised RGB image based salient object detection, RGB-D image pair based salient object detection, weakly supervised salient object detection and camouflaged object detection; 2) we analyze the connection between the transformer network and the salient object detection task and demonstrate that the transformer backbone is extremely powerful in the context-based tasks, *e.g.*, salient object detection, camouflaged object detection; 3) we design a very simple decoder for the three fully supervised tasks, and adopt Gated-CRF loss [23] and a self-supervised learning strategy to the weakly supervised task, leading to new benchmark for the fully supervised tasks, and significantly improved performance for the weakly supervised model, which is even comparable or outperforms the existing convolutional neural network based fully supervised salient object detection models.

## 2 RELATED WORK

In this section, we will introduce the existing SOD and COD models, and recent work on transformer network.

### RGB Image based Fully Supervised Salient Object Detection:

As discussed above, existing fully supervised RGB image based salient object detection models [1, 2, 13, 14, 17, 24] mainly focus on designing effective decoder to achieve high-low level feature aggregation. Wu *et al.* [1] proposes a “Stacked Cross Refinement Network”, and uses the interaction between the edge module and the detection module to optimize the two tasks at the same time. We *et al.* [2] introduces an adaptive selection of complementary information when aggregating multi-scale features, and presents a structure-aware loss function, which solves the problem of differences in multi-scale features during fusion. Qin *et al.* [25] uses multiple supervisions and high-quality boundaries to guide the encoder, decoder and residual refinement module to gradually optimize the saliency prediction to obtain a more refined segmentation. [26] integrates the information of adjacent layers, and integrates multi-scale information to retain the internal consistency of each category (salient foreground or non-salient background).

**RGB Image based Weakly Supervised Salient Object Detection:** The weakly supervised saliency models [5, 6, 9, 27, 28, 29] learn saliency from easy-to-obtain weak labels, including image-level labels [6, 27], noisy labels [8, 9, 30] or partial scribble

labels [5, 28]. Due to the limited structure information in the weak annotations, the performance of existing weakly supervised models is still far from satisfactory, and the main focus of existing weakly supervised salient object detection models is to recover the structure information by designing the pair-wise constraints related regularizer.

**RGB-D Image Pair based Fully Supervised Salient Object Detection:** As there exists the depth data in the RGB-D image pair, one of the main focuses of the fully supervised RGB-D image pair based salient object detection models is to explore the complementary information between the RGB image and the depth data. Depending on how information from these two modalities is fused, existing RGB-D salient object detection models can be divided into three categories: early-fusion models [3, 31], late-fusion models [32, 33, 34] and cross-level fusion models [4, 35, 36, 37, 38, 39, 40, 41, 42, 43, 44, 45, 46]. The early-fusion models fuse RGB image and depth data in the input layer, forming a four-channel feature map. The late fusion models treat each mode (RGB and depth) separately, and then saliency fusion is achieved at the output layer. The cross-level fusion models gradually fuse feature of RGB and depth [4, 40, 41, 43, 45, 46, 47, 48, 49].

**Camouflaged Object Detection:** Camouflaged object detection is an important biological phenomenon that animals attempt to hide into the surroundings and thus deceive the viewers [50]. In early studies, the camouflaged object detection is defined as contrast based task, where the contrast computed by the hand-crafted features, such as edges, brightness, corner points and texture to separate the camouflaged object and the background [51, 52, 53, 54, 55]. However, the manual features are vulnerable to the attack from the sophisticated camouflage strategies. Therefore, the recent research turns to the deep learning to incorporate more structure information about the object for detection. Le *et al.* [56] proposes to employ an auxiliary classification network to discriminate the images containing the camouflaged objects and segment the objects through the segmentation network. Fan *et al.* [57] constructs SINet that composed of a search module to search the candidate regions and an identification module for precise localization. Ren *et al.* [58] formulates texture-aware refinement modules and emphasizing the difference between the texture-aware features. Dong *et al.* [59] uses a significant large receptive field to provide rich context information and an effective fusion strategy to aggregate features with different levels of representation.

**Transformer Network and its Application:** Transformer [21] is a set-to-set method based on self-attention mechanism, which achieved great success in natural language processing (NLP). The breakthroughs from Transformer networks in NLP domain has sparked great interest in the computer vision community to adapt these models for vision tasks such as object detection [60, 61, 62, 63, 64], image segmentation [22, 63, 65], object tracking [66, 67, 68], pose estimation [69, 70], optical flow [71] etc.. The dense prediction tasks aim to perform pixel-level classification or regression on the feature map. In recent years, dense prediction tasks usually usefully convolutional neural networks (FCNs), which adopt convolution and sub-sampling with different feature attention or enhancement methods as their fundamental elements in order to learn multi-scale representations. Inspired by the success of Vision Transformer(ViT)[72] in the task of image classification, some works extend such classification model as a backbone for dense prediction tasks. SETR [65] directly

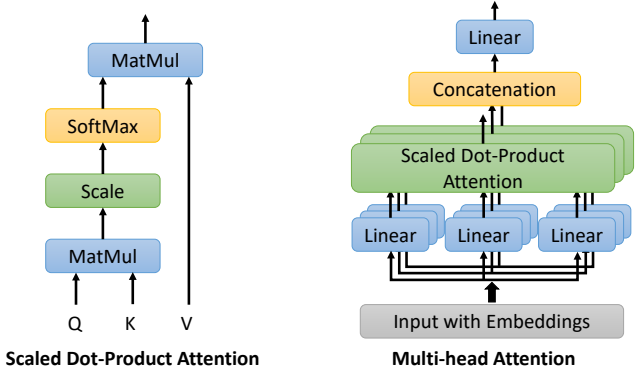


Fig. 3. “Multi-Head Attention” consists of several “Scaled Dot-Product Attention” layers running in parallel.

feeds the sequence of image vectors to a standard Transformer encoder, and the decoder is simple several convolutional layers which upsamples feature maps to origin size. PVT [63] is based on the design of ViT, while also maintaining the global receptive field. This method introduces a progressive shrinking pyramid to reduce the sequence length of the transformer when the network depth increases, thereby significantly reducing the amount of calculation. DPT [22] uses a U-shape structure, which uses ViT as encoder to encode features from different spatial resolutions of the initial embedding throughout all transformer stages. And a decoder assembles the set of tokens into image-like feature representations at various resolutions. Such feature representations are progressively fused into the final dense prediction.

### 3 OUR METHOD

In this section, we will first introduce the transformer backbone, and analyze the connection between transformer networks and the salient object detection and camouflage object detection tasks. We then apply the transformer backbone to three salient object detection tasks and one camouflaged object detection task.

#### 3.1 Transformer Network: An Overview

**Multi-Head Self Attention:** The typical idea in transformer networks is self-attention, which captures long-term dependencies between elements in an input sequence. The self-attention mechanism aims to estimate the relevance of one item to other items in a given sequence, which explicitly models the interactions between all items of a sequence.

We denote a sequence  $\mathbf{X} \in \mathbb{R}^{n \times d}$ , where  $n$  is the sequence length and  $d$  is the embedding dimension as input vector. The input vector is first transformed into three different vectors: the query vector  $\mathbf{Q}$ , the key vector  $\mathbf{K}$  and the value vector  $\mathbf{V}$  with the same dimension  $d$ . This is done by defining three learnable weight matrices  $\mathbf{W}^Q \in \mathbb{R}^{n \times d_q}$ ,  $\mathbf{W}^K \in \mathbb{R}^{n \times d_k}$  and  $\mathbf{W}^V \in \mathbb{R}^{n \times d_v}$ . The input sequence  $X$  is projected onto these weight matrices to get:

$$\mathbf{Q} = \mathbf{XW}^Q, \mathbf{K} = \mathbf{XW}^K, \mathbf{V} = \mathbf{XW}^V. \quad (1)$$

Based on the above three weight matrices, we compute the dot-product of the query with all keys. Then the results are normalized into attention scores using the softmax operator. Finally, each value vector is multiplied by the sum of the attention scores. In this way, vectors with larger attention scores receive additional focus

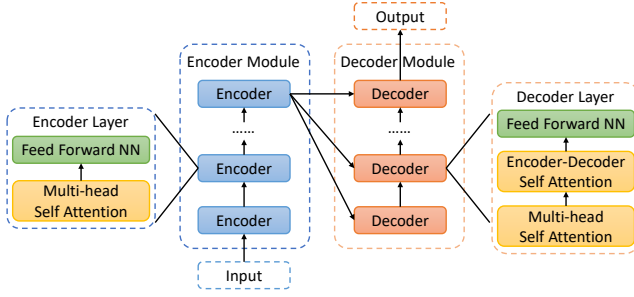


Fig. 4. The structure of vanilla Transformer.

from the following layers. The definition of scaled dot-product self-attention is:

$$\mathbf{Z} = \text{softmax}\left(\frac{\mathbf{Q}\mathbf{K}^T}{\sqrt{d}}\right)\mathbf{V}. \quad (2)$$

The output of the self-attention layer is independent of the input order. To solve the missing positional information of input vectors, an additional positional encoding is added to the inputs. There are two optional encoding forms, including learnable parameters and sine/cosine functions encoding. The form of the latter is as follows:

$$\begin{aligned} \mathbf{PE}(pos, 2i) &= \sin\left(\frac{pos}{10000^{\frac{2i}{d}}}\right), \\ \mathbf{PE}(pos, 2i + 1) &= \cos\left(\frac{pos}{10000^{\frac{2i}{d}}}\right), \end{aligned} \quad (3)$$

where  $pos$  is the position of the word in a vector and  $i$  is the dimension of the positional encoding, thus each dimension of the positional encoding corresponds to a sinusoid.

The self-attention is then extended to multi-head self-attention to perform the self-attention layer in parallel. Specifically, as shown in Fig. 3, to project the inputs into different representations, different weight matrices are used for different heads. Features then pass through the multi-head attention layer, and are concatenated to get the final results by another linear projection.

**Transformer Network:** In Fig. 4, the Transformer [21] is composed of a multi-layer encoder module and a multi-layer decoder module, which was firstly applied on the machine translation task in neural language processing (NLP). Each encoder is composed of a multi-head self attention layer and a feed-forward network, while each decoder is composed of a multi-head self attention layer, an encoder-decoder attention layer and a feed-forward network [73].

**Image Transformer:** We extend the above basic transformer structure to process 2D images, which was firstly used in ViT [72]. To adapt such a framework, a straightforward method is to flatten the input image with size of  $H \times W \times 3$  into a 1D vector with size of  $3HW$ . However, this will lead to excessive computational complexity since the vector length of a flattened image is too long and the computational complexity of multi-head self-attention is  $O(N)$ .

In order to maintain a small amount of calculation while completing serialization modeling, we first use a ResNet-50 [16] to downsample the input image to a high-level feature map with size  $\frac{H}{16} \times \frac{W}{16} \times 3$ , and then divide the feature map into patches with size of  $1 \times 1$ , which means  $\frac{H}{16}$  and  $\frac{W}{16}$  of original image size. In this way, the input image can be viewed as a sequence with length

of  $\frac{HW}{256}$ . So we flatten such divided patches into a sequence and use a trainable liner projection function to map the original patch sequence to embedding space. In this way, we can use the image transformer to process 2D image data, which will greatly improve the performance of salient object detection.

### 3.2 Transformer based Salient Object Detection

Visual salient object detection is a context based task [12], and we define salient objects as those that stand out from their surroundings with high contrast as shown in Fig. 6. Usually, salient objects have both high global contrast and local contrast compared with its neighbourhood. Conventional handcrafted-feature based methods [10, 11] compute the saliency of each pixel by comparing the contrast of each pixel with all the other pixels, which lead to both global and local contrast information modeling. The early deep convolutional network based saliency models [74] mimic the contrast modeling strategy, but they use deep features from convolutional neural networks instead of handcrafted features. The highly representative deep features lead to significant performance improvement of such deep saliency models [1, 2, 14, 17].

We argue that the local connection feature of convolutional neural networks makes it less effective in exploring the long-range dependency of saliency. We roughly visualize the receptive field of convolutional neural network in Fig. 1, which indicates that convolutional neural networks can only achieve local context modeling instead of global context modeling, which is essential for the context based tasks, *e.g.*, salient object detection in particular.

Due to the high effectiveness of transformer networks [21] in long-range dependency modeling, we introduce the transformer backbone [22] based salient object detection network as shown in Fig. 5 for fully supervised salient object detection and Fig. 7 for weakly supervised salient object detection. Let's define our training dataset as  $D = \{x, y\}_{i=1}^N$ , where  $x$  is the input RGB image or RGB-D image pair,  $y$  is the corresponding ground truth map or scribble based weak supervision. We design both our fully supervised and weakly supervised model with the dense transformer backbone [22] (the res50 version in particular), and we define the four stages of features from the transformer backbone as  $s_1, s_2, s_3$  and  $s_4$ , where each stage of feature has the same channel size, which is 256. The downsampling rates are 1/4, 1/8, 1/16 and 1/32 respectively for each stage of feature.

#### 3.2.1 Fully supervised model

We introduce two fully supervised transformer backbone [21] based models, namely RGB salient object detection and RGB-D salient object detection. We perform early fusion for the RGB-D salient object detection model, and concatenate RGB image and depth data in the input layer, which leads to a four channel feature map. Then, we feed it to a  $3 \times 3$  convolutional layer to obtain a three-channel feature map, and feed it to the "Transformer Encoder" in Fig. 5. For RGB salient object detection, we directly feed the RGB image to the "Transformer Encoder".

As each level of the "Transformer Encoder" has already encoded long-range dependency, a simple decoder is introduced as shown in Fig. 5 to aggregate features of different levels of network. Specifically, we first upsample  $\{s_k\}_{k=1}^4$  to same spatial size which is 1/4 of the original image size. Then, we concatenate them and obtain a new feature map  $s_s$  of channel size  $256 \times 4$ . To obtain discriminative channel-wise features, we feed  $s_s$  to a residual channel attention module [75] to obtain  $s'_s$  of same size

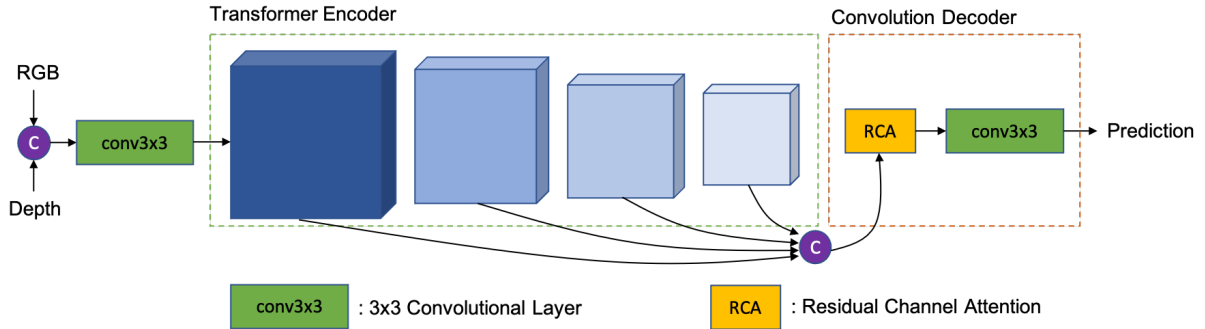


Fig. 5. Network structure of the fully supervised models. For RGB salient object detection and RGB camouflage detection, we directly feed the input RGB image to the “Transformer Encoder”. For RGB-D salient object detection, we concatenate RGB and depth in the input layer, and feed it to a  $3 \times 3$  convolutional layer to obtain a three-channel feature map, which is then feed to the “Transformer Encoder”.

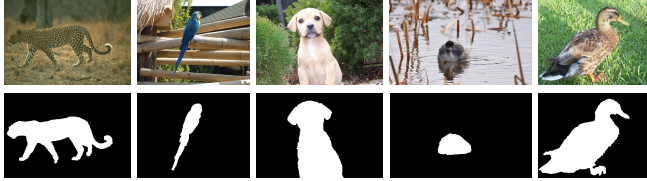


Fig. 6. Images (1<sup>st</sup> row) and the corresponding saliency maps (2<sup>nd</sup> row).

as  $s_s$ . Then one  $3 \times 3$  convolutional layer is used to map  $s_s'$  to a one-channel saliency map  $c$  (a four-times upsampling is used to achieve  $c$  of same spatial size as  $x$ ).

To train the fully supervised model, the weighted structure-aware loss [2] is adopted, which is the sum of weighted binary cross-entropy loss and weighted IOU loss as:

$$\mathcal{L}_{full}(c, y) = \omega * \mathcal{L}_{ce}(c, y) + \mathcal{L}_{iou}(c, y), \quad (4)$$

where  $\omega$  is the edge-aware weight, which is defined as  $\omega = 1 + 5 * |(\text{avg\_pool}(y) - y)|$ ,  $\mathcal{L}_{ce}$  is the binary cross-entropy loss,  $\mathcal{L}_{iou}$  is the weighted IOU loss, which is defined as:

$$\mathcal{L}_{iou} = 1 - \frac{\omega * \text{inter} + 1}{\omega * \text{union} - \omega * \text{inter} + 1}, \quad (5)$$

where  $\text{inter} = c * y$ , and  $\text{union} = c + y$ .

Due to the similarity of camouflaged object detection and salient object detection, we also perform fully supervised COD in this paper, which leads to three fully supervised models in total, namely fully supervised RGB salient object detection, RGB-D salient object detection and RGB camouflage detection. Note that, we use the same network structure as in Fig. 5 and same loss function as in Eq. (4) for all these three tasks, except that we map the concatenation of RGB image and depth to a three-channel feature map with extra  $3 \times 3$  convolutional layer for the RGB-D salient object detection task.

### 3.2.2 Weakly supervised model

We also design a weakly supervised salient object detection network as shown in Fig. 7 to learn saliency from scribble annotation [5]. Different from full annotations with annotation for each pixel, the scribble annotation only highlights part of the foreground or background region as shown in Fig. 8. As there exists no structure information in scribble annotation, following [5, 28], we design an “Edge Detection Module”, same as [5], and adopt the smoothness

loss [76] to recover the missing structure information. Further, inspired by [28], we adopt the Gated-CRF loss [23] to model the pair-wise constraints of model prediction based on the assumption that nearby pixels should have similar saliency predictions. Lastly, we introduce a self-supervised learning strategy to our network to achieve scale-invariant predictions.

Particularly, we feed the RGB image to the transformer backbone based weakly supervised learning network as shown in Fig. 7. Following the fully supervised network, we have the same “Transformer Encoder” and “Convolution Decoder” in the weakly supervised learning pipeline to generate initial prediction “Prediction#1”. Then, we have an “Edge Detection Module” [5] to map features from different stages of the network to a one-channel edge map  $e$ . To further recover the structure information of “Prediction#1”, we map  $e$  and “Prediction#1” to feature maps of channel size  $M = 32$ , and then concatenate them channel-wise. A residual channel attention [75] is used to obtain discriminative feature representation. Finally, a  $3 \times 3$  convolutional layer is used to map the concatenated feature to an one channel saliency map “Prediction#2”.

As mentioned above, we have three different loss functions for each prediction, namely the partial cross-entropy loss  $\mathcal{L}_{pce}$  to constrain the accuracy in the labeled region, the smoothness loss  $\mathcal{L}_{sm}$  to achieve predictions with the edges well-aligned with the input image, the Gated-CRF loss  $\mathcal{L}_{gcrf}$  for pair-wise term relationship modeling, the self-supervised loss  $\mathcal{L}_{ss}$  to achieve scale-invariant predictions. Further, we have the edge loss for the “Edge Detection Module” to produce a salient edge map, and further constrain the model prediction. To generate supervision for the “Edge Detection Module”, we define the gradient map of the model prediction  $\partial \text{Prediction}\#1$  as a pseudo ground truth edge map, and define the edge loss as binary cross-entropy loss  $\mathcal{L}_{ce}(e, \partial \text{Prediction}\#1)$ .

In this way, the final loss function for the weakly supervised learning pipeline is defined as:

$$\mathcal{L}_{weak} = \mathcal{L}_{\text{Prediction}\#1} + \mathcal{L}_{\text{Prediction}\#2} + \lambda \mathcal{L}_{ce}(e, \partial \text{Prediction}\#1), \quad (6)$$

where  $\lambda$  is used to control the contribution of edge loss, and empirically we define  $\lambda = 1$ .  $\mathcal{L}_{\text{Prediction}\#1}$  and  $\mathcal{L}_{\text{Prediction}\#2}$  are loss functions for  $\text{Prediction}\#1$  and  $\text{Prediction}\#2$  respectively, which have the same loss components as:

$$\mathcal{L}_{\text{Prediction}\#1} = \mathcal{L}_{pce} + \lambda_1 * \mathcal{L}_{sm} + \lambda_2 * \mathcal{L}_{gcrf} + \lambda_3 * \mathcal{L}_{ss}. \quad (7)$$

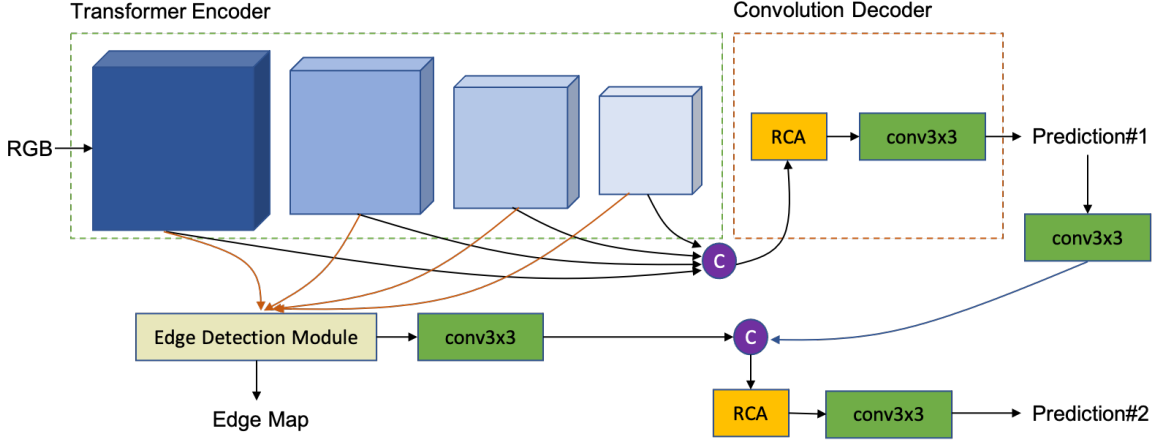


Fig. 7. Network structure of the weakly supervised models, where the “Edge Detection Module” is same as the edge module in [5].



Fig. 8. Scribble annotations label part of foreground/background region, where the yellow scribble indicates the salient foreground, and blue scribble shows the background region.

Empirically, we set the loss weights as  $\lambda_1 = 0.3$ ,  $\lambda_2 = 1$  and  $\lambda_3 = 0.3$ . For the self-supervised loss, we resize the image  $x$  to half of its original scale to obtain prediction  $c_h$ . We then define the self-supervised loss as a weighted sum of the structural similarity index measure and L1 loss following [28], which is defined as:

$$\mathcal{L}_{ss} = \alpha * SSIM(c_h, c) + (1 - \alpha) * L1(c_h, c). \quad (8)$$

We set  $\alpha = 0.85$  in our experiments.

## 4 EXPERIMENTAL RESULTS

### 4.1 Task Introduction

For static image based salient object detection, we perform experiments on RGB salient object detection, RGB-D salient object detection and weakly supervised RGB salient object detection, which covers both fully supervised saliency segmentation and weakly supervised saliency segmentation. For camouflaged object detection, we only conduct experiments on fully supervised RGB image based camouflaged object detection.

### 4.2 Setup

**Dataset:** For the salient object detection task, we train the models by using DUTS training dataset [6], and test on six other widely used data sets: the DUTS testing dataset, ECSSD [78], DUT [11], HKU-IS [74], PASCAL-S [79] and the SOD testing dataset [80]. For weakly supervised RGB image based salient object detection, we train our model using the DUTS-S training dataset [5] with scribble annotations, and testing on above six benchmark RGB saliency testing dataset. For the camouflaged object detection task, we train the models using the COD10K training dataset [57], and test them on four test datasets: CAMO [56], CHAMELEON [83], the COD10K testing dataset, and NC4K [84]. For RGB-D salient object detection models, we follow the conventional

training setting, in which the training set is a combination of 1,485 images from the NJU2K dataset [85] and 700 images from the NLPR dataset [86]. We then test the performance of our model and competing models on the NJU2K testing set, NLPR testing set LFSD [87], DES [88], SSB [89] and the SIP [90] testing set.

**Evaluation Metrics:** For all the four tasks, we use four evaluation indicators to measure the performance, including Mean Absolute Error  $\mathcal{M}$ , Mean F-measure ( $F_\beta$ ), Mean E-measure ( $E_\xi$ ) [91] and S-measure ( $S_\alpha$ ) [92].

**MAE**  $\mathcal{M}$  is defined as the pixel-wise difference between the predicted  $c$  and the pixel-wise binary ground-truth  $y$ :

$$\text{MAE} = \frac{1}{H \times W} |c - y|, \quad (9)$$

where  $H$  and  $W$  are the height and width of  $c$  correspondingly.

**F-measure**  $F_\beta$  is a region based similarity metric, and we provide the mean F-measure using varying fixed (0-255) thresholds.

**E-measure**  $E_\xi$  is the recent proposed Enhanced alignment measure [91] in the binary map evaluation field to jointly capture image-level statistics and local pixel matching information.

**S-measure**  $S_\alpha$  is a structure based measure [92], which combines the region-aware ( $S_r$ ) and object-aware ( $S_o$ ) structural similarity as their final structure metric:

$$S_\alpha = \alpha S_o + (1 - \alpha) S_r, \quad (10)$$

where  $\alpha \in [0, 1]$  is the balance parameter and set to 0.5 as default.

**Implementation Details:** We train our model in Pytorch with the dense transformer backbone [22], which is initialized with weights trained on [72], and other newly added layers are randomly initialized. We resize all the images and ground truth to  $352 \times 352$ . The maximum epoch is 30. The initial learning rates are  $2.5 \times 10^{-5}$  for all the four tasks in this paper. The whole training takes 9 hours, 10 hours, 2.5 hours and 3 hours with batch size 6 on one NVIDIA GTX 2080Ti GPUs for fully supervised RGB SOD, weakly supervised RGB SOD, RGB-D image pair based SOD and COD task respectively.

We use the same network structure for all the fully supervised tasks, except that when the depth data is available, we feed the concatenation of the RGB image and depth to a  $3 \times 3$  convolutional layer to obtain a three channel feature map, which is then feed to the transformer backbone. For weakly supervised learning, we introduce an extra edge detection module [5], smoothness loss

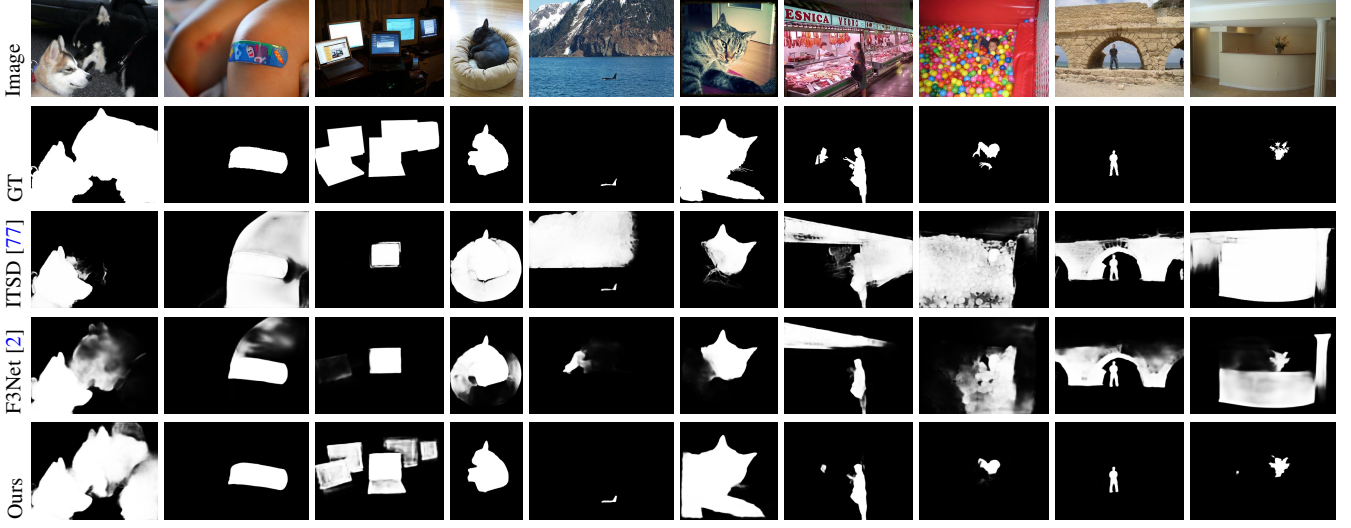


Fig. 9. Predictions from two state-of-the-art RGB salient object detection models and our transformer backbone based model.

TABLE 1  
Performance comparison with benchmark RGB salient object detection models.

Method	DUTS [6]				ECSSD [78]				DUT [11]				HKU-IS [74]				PASCAL-S [79]				SOD [80]			
	$S_\alpha \uparrow$	$F_\beta \uparrow$	$E_\xi \uparrow$	$\mathcal{M} \downarrow$	$S_\alpha \uparrow$	$F_\beta \uparrow$	$E_\xi \uparrow$	$\mathcal{M} \downarrow$	$S_\alpha \uparrow$	$F_\beta \uparrow$	$E_\xi \uparrow$	$\mathcal{M} \downarrow$	$S_\alpha \uparrow$	$F_\beta \uparrow$	$E_\xi \uparrow$	$\mathcal{M} \downarrow$	$S_\alpha \uparrow$	$F_\beta \uparrow$	$E_\xi \uparrow$	$\mathcal{M} \downarrow$	$S_\alpha \uparrow$	$F_\beta \uparrow$	$E_\xi \uparrow$	$\mathcal{M} \downarrow$
Fully-supervised SOD Models																								
CPD [17]	.869	.821	.898	.043	.913	.909	.937	.040	.825	.742	.847	.056	.906	.892	.938	.034	.848	.819	.882	.071	.799	.779	.811	.088
SCRN [1]	.885	.833	.900	.040	.920	.910	.933	.041	.837	.749	.847	.056	.916	.894	.935	.034	.869	.833	.892	.063	.817	.790	.829	.087
PoolNet [81]	.887	.840	.910	.037	.919	.913	.938	.038	.831	.748	.848	.054	.919	.903	.945	.030	.865	.835	.896	.065	.820	.804	.834	.084
BASNet [25]	.876	.823	.896	.048	.910	.913	.938	.040	.836	.767	.865	.057	.909	.903	.943	.032	.838	.818	.879	.076	.798	.792	.827	.094
EGNet [82]	.878	.824	.898	.043	.914	.906	.933	.043	.840	.755	.855	.054	.917	.900	.943	.031	.852	.823	.881	.074	.824	.811	.843	.081
F3Net [2]	.888	.852	.920	.035	.919	.921	.943	.036	.839	.766	.864	.053	.917	.910	.952	.028	.861	.835	.898	.062	.824	.814	.850	.077
ITSD [77]	.886	.841	.917	.039	.920	.916	.943	.037	.842	.767	.867	.056	.921	.906	.950	.030	.860	.830	.894	.066	.836	.829	.867	.076
Ours	<b>.910</b>	<b>.891</b>	<b>.946</b>	<b>.027</b>	<b>.940</b>	<b>.945</b>	<b>.967</b>	<b>.023</b>	<b>.870</b>	<b>.824</b>	<b>.905</b>	<b>.042</b>	<b>.929</b>	<b>.928</b>	<b>.965</b>	<b>.023</b>	<b>.870</b>	<b>.871</b>	<b>.914</b>	<b>.056</b>	<b>.852</b>	<b>.862</b>	<b>.892</b>	<b>.064</b>
Weakly-supervised SOD Models																								
SSAL [5]	.803	.747	.865	.062	.863	.865	.908	.061	.785	.702	.835	.068	.865	.858	.923	.047	.798	.773	.854	.093	.750	.743	.801	.108
WSS [6]	.748	.633	.806	.100	.808	.774	.801	.106	.730	.590	.729	.110	.822	.773	.819	.079	.701	.691	.687	.187	.698	.635	.687	.152
C2S [29]	.805	.718	.845	.071	-	-	-	-	.773	.665	.810	.082	.869	.837	.910	.053	.784	.806	.813	.130	.770	.741	.799	.117
SCWS [28]	.841	.818	.901	.049	.879	.894	.924	.051	.813	.751	.856	.060	.883	.892	.938	.038	.821	.815	.877	.078	.782	.791	.833	.090
Ours	<b>.867</b>	<b>.833</b>	<b>.926</b>	<b>.040</b>	<b>.910</b>	<b>.917</b>	<b>.952</b>	<b>.035</b>	<b>.842</b>	<b>.780</b>	<b>.888</b>	<b>.054</b>	<b>.906</b>	<b>.902</b>	<b>.956</b>	<b>.031</b>	<b>.853</b>	<b>.836</b>	<b>.903</b>	<b>.062</b>	<b>.821</b>	<b>.825</b>	<b>.877</b>	<b>.078</b>

[76], Gated-CRF loss [23] and self-supervised loss as in Eq. (8) to the partial cross-entropy loss to recover the missing structure information in scribble annotations following [5, 28].

### 4.3 RGB image based models

For RGB image based models, we investigate RGB image salient object detection, weakly supervised RGB image salient object detection and camouflaged object detection.

#### 4.3.1 Saliency/Camouflage Detection

As a context based task, the existing salient object detection models aim to identify and segment image parts that attract human visual attention. Specifically, the SOD models focus on effectively aggregating features of different stages of the backbone network to achieve fine-grained predictions. However, when the salient target is more complex, the existing SOD models also fail to segment the complete object as shown in Fig. 9. Further, the lost information in the encoder part will never be restored in the refinement process. We argue that the existing backbones, *e.g.*, VGG16 [15], ResNet50 [16], may fail to encode the global context information for salient object detection, leading to less effective models. We introduce the transformer backbone [22] to salient object detection to obtain

global context information at each stage of network, and achieve better performance as shown in both Fig. 9 “Ours” and Table 1 “Ours” of the “Fully-supervised SOD Models” section.

Similar to SOD, COD is also a context based task, as the prey evolves to have similar pattern as its surrounding to avoid being recognized by predators. The goal of camouflaged object detection model is to identify and segment objects that are camouflaged in the environment. Since camouflaged objects share similar texture and structure information with the background, camouflaged objects are harder to recognize than salient object changes. The existing camouflaged object detection techniques [57, 84, 94] design camouflaged object detection networks with convolutional neural network following a similar pipeline as salient object detection, which usually involves an encoder to extract camouflage features, and a decoder to aggregate features from different levels of network to produce an one channel camouflage map. Due to the smaller receptive field of those models, the existing techniques fail to identify camouflaged objects when they share too similar pattern to their surroundings as shown in Fig. 10 “SINet[57]”. The transformer backbone based camouflaged object detection network is effective in long-range dependency modeling, which can reveal the global context information for effective camouflaged object

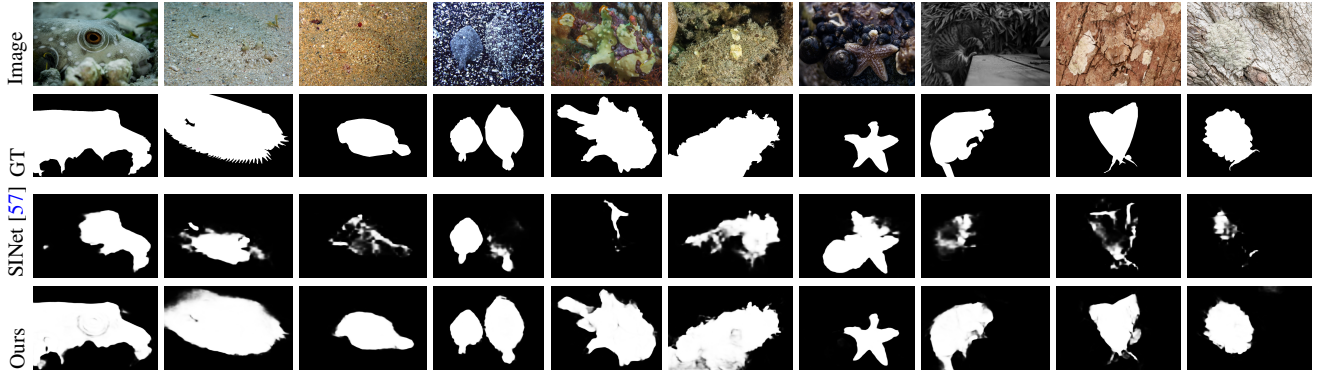


Fig. 10. Predictions of the state-of-the-art camouflaged object detection model (SINet [57]) and our transformer backbone based model.

TABLE 2  
Performance comparison with benchmark camouflaged object detection models.

Method	CAMO [56]				CHAMELEON [83]				COD10K [57]				NC4K [84]			
	$S_\alpha \uparrow$	$F_\beta \uparrow$	$E_\xi \uparrow$	$\mathcal{M} \downarrow$	$S_\alpha \uparrow$	$F_\beta \uparrow$	$E_\xi \uparrow$	$\mathcal{M} \downarrow$	$S_\alpha \uparrow$	$F_\beta \uparrow$	$E_\xi \uparrow$	$\mathcal{M} \downarrow$	$S_\alpha \uparrow$	$F_\beta \uparrow$	$E_\xi \uparrow$	$\mathcal{M} \downarrow$
SCRN [1]	.779	.705	.796	.090	.876	.787	.889	.042	.789	.651	.817	.047	.832	.759	.855	.059
CSNet[93]	.771	.705	.795	.092	.856	.766	.869	.047	.778	.635	.810	.047	.819	.748	.845	.061
SINet [57]	.745	.702	.804	.092	.872	.827	.936	.034	.776	.679	.864	.043	.810	.772	.873	.057
LSR [84]	.793	.725	.826	.085	.893	.839	.938	.033	.793	.685	.868	.041	.839	.779	.883	.053
UJSC [94]	.803	.759	.853	.076	.894	.848	.943	.030	.817	.726	.892	.035	-	-	-	-
Ours	<b>.846</b>	<b>.832</b>	<b>.913</b>	<b>.051</b>	<b>.904</b>	<b>.875</b>	<b>.956</b>	<b>.022</b>	<b>.838</b>	<b>.774</b>	<b>.921</b>	<b>.027</b>	<b>.876</b>	<b>.856</b>	<b>.934</b>	<b>.033</b>

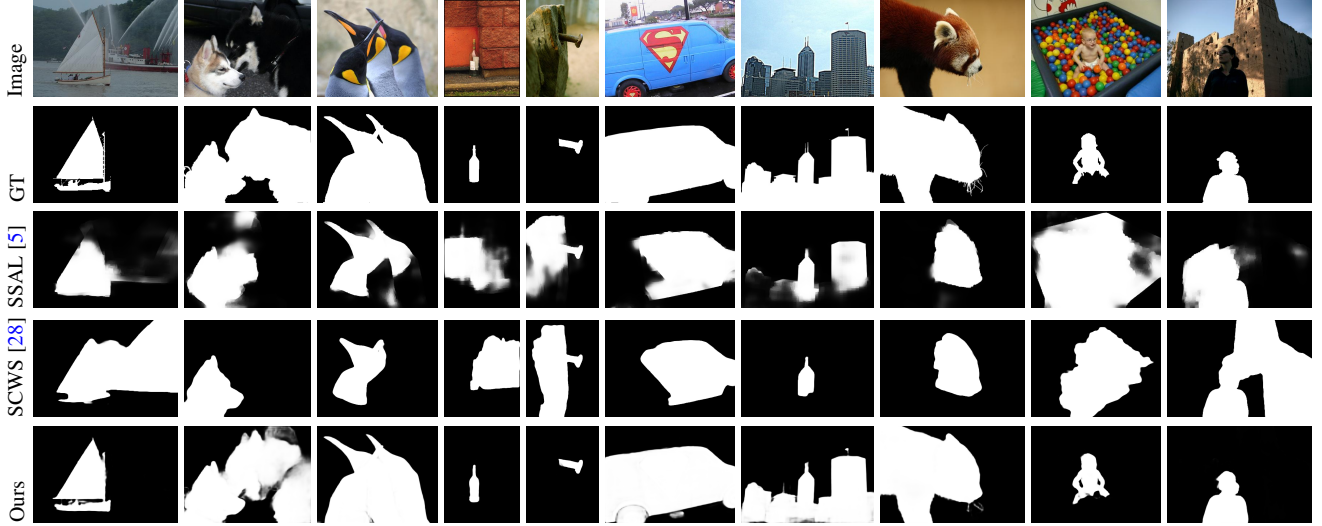


Fig. 11. Predictions of the state-of-the-art weakly supervised salient object detection models (SSAL [5] and SCWS [28]) and our transformer backbone based model.

detection as shown in Fig. 10 “Ours” and Table 2 “Ours”.

#### 4.3.2 Weakly-supervised Salient Object Detection Model

Following [5, 28], we design a transformer backbone [22] based weakly supervised salient object detection model as shown in Fig. 7 to learn saliency from scribble annotations, and the performance is shown in Table 1 “Ours” in the “Weakly-supervised SOD Models” section, which clearly show the superior performance of the proposed model. Further, we show some failure cases of [5, 28] and our corresponding predictions in Fig. 11, which explains that our transformer backbone based weakly supervised model can produce accurate predictions with sharp object boundaries.

#### 4.4 RGB-D based Models

For RGB-D based models, we only investigate RGB-D salient object detection, and design a similar network as the RGB salient object detection model, except that we concatenate RGB image and depth data in the input layer and feed it to a  $3 \times 3$  convolutional layer to obtain a feature map of channel size 3, which is then fed to the “Transformer Encoder” in Fig. 5. The performance of our transformer backbone based RGB-D salient object detection model is shown in Table 3, which clearly verifies the effectiveness of our solution. We also show failure cases of the state-of-the-art models and our corresponding predictions in Fig. 12, which further demonstrate the superiority of our network.

TABLE 3  
Performance comparison with benchmark RGB-D salient object detection models.

Method	NJU2K [85]				SSB [89]				DES [88]				NLPR [86]				LFSD [87]				SIP [90]			
	$S_\alpha \uparrow$	$F_\beta \uparrow$	$E_\xi \uparrow$	$\mathcal{M} \downarrow$	$S_\alpha \uparrow$	$F_\beta \uparrow$	$E_\xi \uparrow$	$\mathcal{M} \downarrow$	$S_\alpha \uparrow$	$F_\beta \uparrow$	$E_\xi \uparrow$	$\mathcal{M} \downarrow$	$S_\alpha \uparrow$	$F_\beta \uparrow$	$E_\xi \uparrow$	$\mathcal{M} \downarrow$	$S_\alpha \uparrow$	$F_\beta \uparrow$	$E_\xi \uparrow$	$\mathcal{M} \downarrow$	$S_\alpha \uparrow$	$F_\beta \uparrow$	$E_\xi \uparrow$	$\mathcal{M} \downarrow$
BBSNet [4]	.921	.902	.938	.035	.908	.883	.928	.041	.933	.910	.949	.021	.930	.896	.950	.023	.864	.843	.883	.072	.879	.868	.906	.055
BiaNet [44]	.915	.903	.934	.039	.904	.879	.926	.043	.931	.910	.948	.021	.925	.894	.948	.024	.845	.834	.871	.085	.883	.873	.913	.052
CoNet [42]	.911	.903	.944	.036	.896	.877	.939	.040	.906	.880	.939	.026	.900	.859	.937	.030	.842	.834	.886	.077	.868	.855	.915	.054
UCNet [3]	.897	.886	.930	.043	.903	.884	.938	.039	.934	.919	.967	.019	.920	.891	.951	.025	.864	.855	.901	.066	.875	.867	.914	.051
JLDCF [95]	.902	.885	.935	.041	.903	.873	.936	.040	.931	.907	.959	.021	.925	.894	.955	.022	.862	.848	.894	.070	.880	.873	.918	.049
Ours	<b>.931</b>	<b>.925</b>	<b>.956</b>	<b>.027</b>	<b>.926</b>	<b>.912</b>	<b>.954</b>	<b>.028</b>	<b>.939</b>	<b>.927</b>	<b>.964</b>	<b>.016</b>	<b>.938</b>	<b>.920</b>	<b>.964</b>	<b>.019</b>	<b>.876</b>	<b>.865</b>	<b>.901</b>	<b>.066</b>	<b>.926</b>	<b>.912</b>	<b>.954</b>	<b>.028</b>

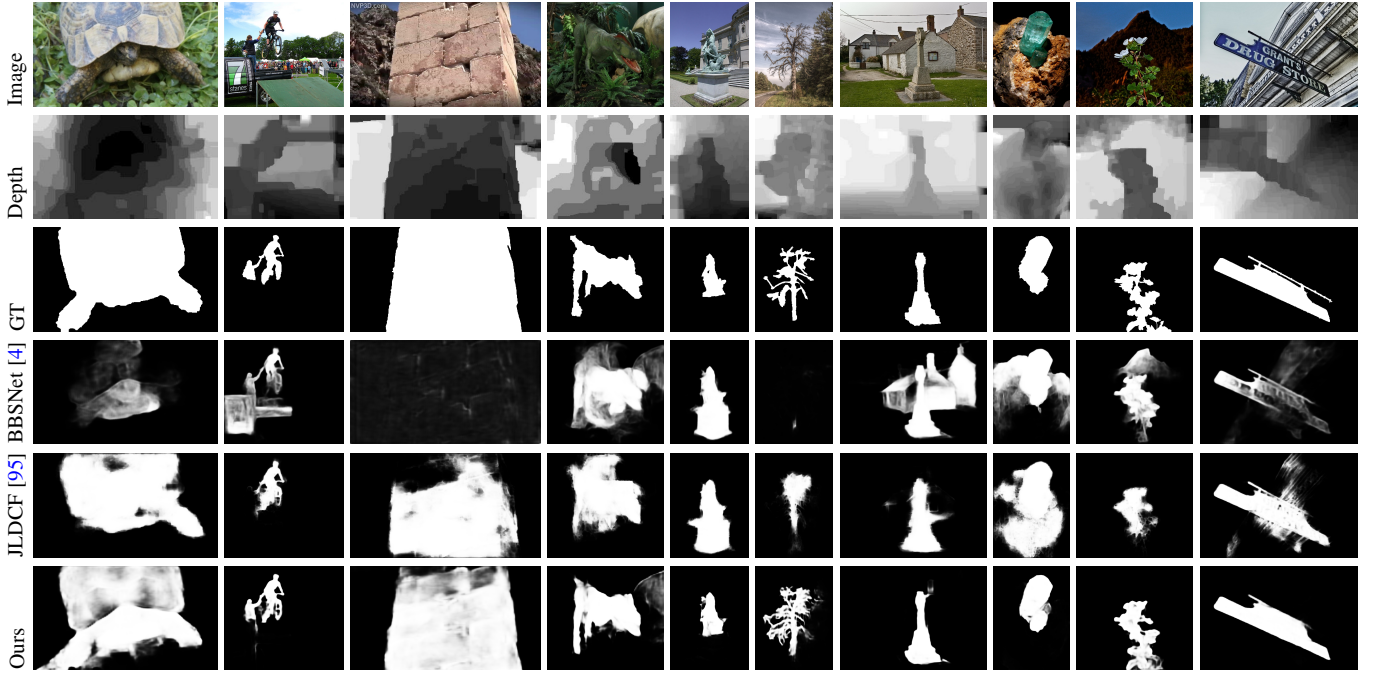


Fig. 12. Predictions of the state-of-the-art RGB-D salient object detection models (BBSNet [4] and JLDCF [95]) and our transformer based model.

#### 4.5 Model Analysis

In this section, we analyse our transformer backbone based models in detail. Note that, all the following experiments are based on the fully supervised RGB salient object detection task.

**Model performance w.r.t.learning rate and optimizer:** We observe the transformer backbone based network is sensitive to the initial learning rate. We then analyse the loss convergence of the transformer backbone based network as shown in Fig. 16, which clearly shows that a larger learning rate may lead to significant instability in training. Further, we observe that for the conventional backbone based network, *e.g.*, ResNet50, the SGD optimizer (“ResNet50\_SGD”) and Adam optimizer (“ResNet50\_Adam”) can achieve similar performance as shown in Table 4. However, for the transformer backbone based network, the Adam optimizer (“Ours”) achieves significantly better performance than the model with SGD optimizer (“Ours\_SGD”). We will investigate it further in the future.

**The importance of transformer network as backbone:** We train with same decoder, but change our transformer backbone to VGG16 and ResNet50, and show the model performance in Table 5. The significant performance improvement of our transformer backbone based network further explains the superior performance of our network.

**Model performance with different numbers of training datasets:** We train our transformer backbone networks and

ResNet50 [16] backbone network in Table 5 with different numbers of training datasets, which are 10%, 30%, 50%, 70%, 90% of the entire training dataset respectively, and show model performance in Fig. 14. The consistently better performance of the transformer backbone based model with regard to different numbers of training example explains the effectiveness of our solution. Further, we observe that the mode performance is not always increasing with a larger training dataset, which inspires us to work on active learning based transformer network to actively select representative samples for model training.

**The contribution of transformer, Gated-CRF and self-supervised learning for weakly supervised learning with scribble:** Our weakly supervised salient object detection model is built upon SSAL [5], where we change the VGG16 backbone of SSAL with transformer backbone, and introduce Gated-CRF loss and self-supervised loss as shown in Eq. (7) to the initial loss function in [5]. We then analyze each component and show model performance of each experiment in Table 6, where “SSAL\_T” is [5] with the transformer backbone [22], “SSAL\_T\_G” represents “SSAL\_T” with Gated-CRF loss [23], and “SSAL\_T\_S” is the model of “SSAL\_T” with self-supervised loss function. Table 6 shows that the transformer backbone (“SSAL\_T”) can significant improve weakly supervised learning performance. We also notice that the when we use Gated-CRF loss and self-supervised learning separately, we have limited performance gain, or sometimes, we



Fig. 13. The generated depth for our RGB salient object detection training dataset [6] by using [22].

TABLE 4

Model performance with different optimizer, e.g., SGD and Adam, for the conventional backbone models and our transformer backbone models.

Method	DUTS [6]				ECSSD [78]				DUT [11]				HKU-IS [74]				PASCAL-S [79]				SOD [80]			
	$S_\alpha \uparrow$	$F_\beta \uparrow$	$E_\xi \uparrow$	$\mathcal{M} \downarrow$	$S_\alpha \uparrow$	$F_\beta \uparrow$	$E_\xi \uparrow$	$\mathcal{M} \downarrow$	$S_\alpha \uparrow$	$F_\beta \uparrow$	$E_\xi \uparrow$	$\mathcal{M} \downarrow$	$S_\alpha \uparrow$	$F_\beta \uparrow$	$E_\xi \uparrow$	$\mathcal{M} \downarrow$	$S_\alpha \uparrow$	$F_\beta \uparrow$	$E_\xi \uparrow$	$\mathcal{M} \downarrow$	$S_\alpha \uparrow$	$F_\beta \uparrow$	$E_\xi \uparrow$	$\mathcal{M} \downarrow$
ResNet50_SGD	.873	.838	.913	.038	.917	.918	.948	.035	.816	.750	.859	.056	.914	.910	.950	.030	.849	.845	.900	.067	.825	.820	.859	.075
ResNet50_Adam	.879	.844	.919	.037	.922	.924	.952	.033	.827	.756	.863	.055	.913	.909	.953	.029	.857	.850	.903	.065	.828	.826	.862	.074
Ours_SGD	.890	.856	.916	.036	.923	.914	.948	.034	.846	.769	.872	.053	.920	.908	.957	.030	.861	.836	.905	.067	.833	.841	.871	.075
Ours	<b>.910</b>	<b>.891</b>	<b>.946</b>	<b>.027</b>	<b>.940</b>	<b>.945</b>	<b>.967</b>	<b>.023</b>	<b>.870</b>	<b>.824</b>	<b>.905</b>	<b>.042</b>	<b>.929</b>	<b>.928</b>	<b>.965</b>	<b>.023</b>	<b>.870</b>	<b>.871</b>	<b>.914</b>	<b>.056</b>	<b>.852</b>	<b>.862</b>	<b>.892</b>	<b>.064</b>

TABLE 5  
Performance comparison with different backbone networks for RGB salient object detection

Method	DUTS [6]				ECSSD [78]				DUT [11]				HKU-IS [74]				PASCAL-S [79]				SOD [80]			
	$S_\alpha \uparrow$	$F_\beta \uparrow$	$E_\xi \uparrow$	$\mathcal{M} \downarrow$	$S_\alpha \uparrow$	$F_\beta \uparrow$	$E_\xi \uparrow$	$\mathcal{M} \downarrow$	$S_\alpha \uparrow$	$F_\beta \uparrow$	$E_\xi \uparrow$	$\mathcal{M} \downarrow$	$S_\alpha \uparrow$	$F_\beta \uparrow$	$E_\xi \uparrow$	$\mathcal{M} \downarrow$	$S_\alpha \uparrow$	$F_\beta \uparrow$	$E_\xi \uparrow$	$\mathcal{M} \downarrow$	$S_\alpha \uparrow$	$F_\beta \uparrow$	$E_\xi \uparrow$	$\mathcal{M} \downarrow$
VGG16	.857	.826	.897	.042	.910	.912	.938	.036	.818	.751	.864	.055	.901	.900	.932	.033	.831	.830	.879	.070	.801	.805	.836	.078
ResNet50	.879	.844	.919	.037	.922	.924	.952	.033	.827	.756	.863	.055	.913	.909	.953	.029	.857	.850	.903	.065	.828	.826	.862	.074
Ours	<b>.910</b>	<b>.891</b>	<b>.946</b>	<b>.027</b>	<b>.940</b>	<b>.945</b>	<b>.967</b>	<b>.023</b>	<b>.870</b>	<b>.824</b>	<b>.905</b>	<b>.042</b>	<b>.929</b>	<b>.928</b>	<b>.965</b>	<b>.023</b>	<b>.870</b>	<b>.871</b>	<b>.914</b>	<b>.056</b>	<b>.852</b>	<b>.862</b>	<b>.892</b>	<b>.064</b>

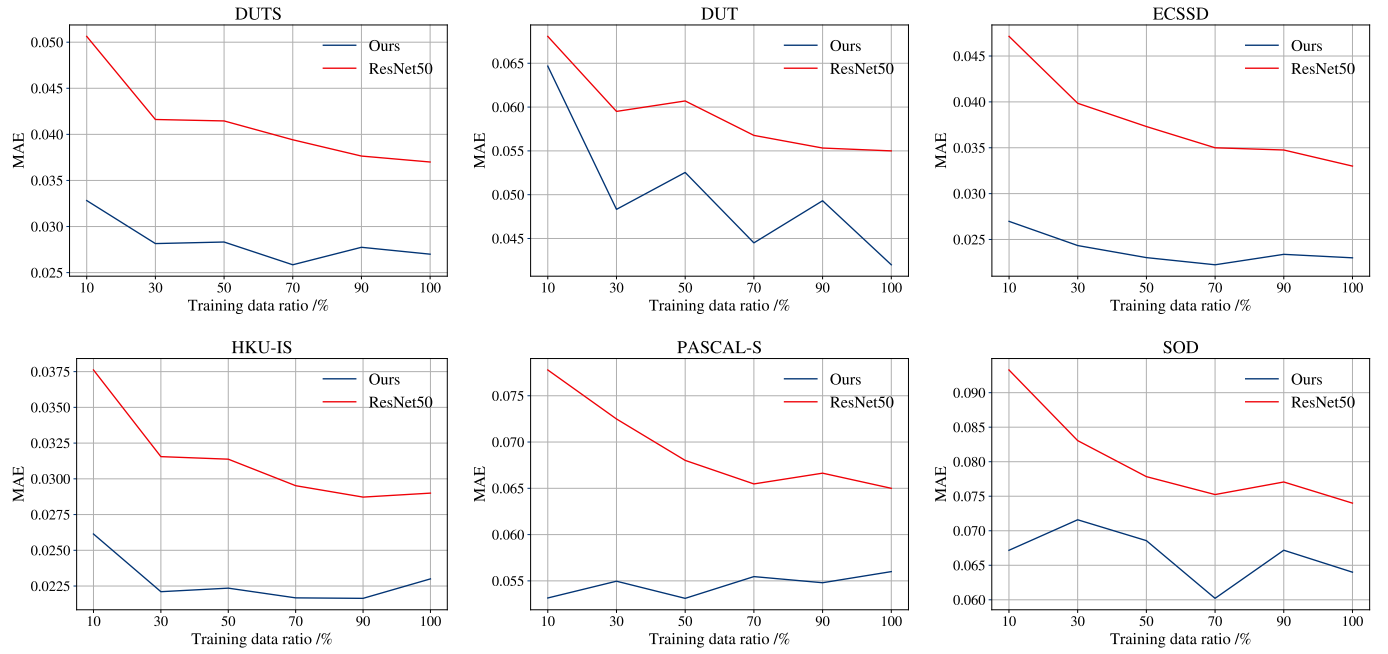


Fig. 14. Model performance of ResNet50 [16] backbone and our transformer backbone based salient object detection network w.r.t. different training dataset sizes on six testing dataset.

even obtain inferior performance than “SSAL\_T”. However, when we use these two loss functions together, we have much better performance (“Ours”) than the transformer backbone network (“SSAL\_T”). The main issue lies in the weight of each loss

function, which will be investigated in the future.

**When does depth help?** Given the trained monocular depth estimation model from [22], we can obtain pseudo depth for our RGB salient object detection training dataset as shown in Fig. 13.

TABLE 6  
Weakly supervised salient object detection model analysis.

Method	DUTS [6]				ECSSD [78]				DUT [11]				HKU-IS [74]				PASCAL-S [79]				SOD [80]			
	$S_\alpha \uparrow F_\beta \uparrow E_\xi \uparrow \mathcal{M} \downarrow$	$S_\alpha \uparrow F_\beta \uparrow E_\xi \uparrow \mathcal{M} \downarrow$	$S_\alpha \uparrow F_\beta \uparrow E_\xi \uparrow \mathcal{M} \downarrow$	$S_\alpha \uparrow F_\beta \uparrow E_\xi \uparrow \mathcal{M} \downarrow$	$S_\alpha \uparrow F_\beta \uparrow E_\xi \uparrow \mathcal{M} \downarrow$	$S_\alpha \uparrow F_\beta \uparrow E_\xi \uparrow \mathcal{M} \downarrow$	$S_\alpha \uparrow F_\beta \uparrow E_\xi \uparrow \mathcal{M} \downarrow$	$S_\alpha \uparrow F_\beta \uparrow E_\xi \uparrow \mathcal{M} \downarrow$	$S_\alpha \uparrow F_\beta \uparrow E_\xi \uparrow \mathcal{M} \downarrow$	$S_\alpha \uparrow F_\beta \uparrow E_\xi \uparrow \mathcal{M} \downarrow$	$S_\alpha \uparrow F_\beta \uparrow E_\xi \uparrow \mathcal{M} \downarrow$	$S_\alpha \uparrow F_\beta \uparrow E_\xi \uparrow \mathcal{M} \downarrow$	$S_\alpha \uparrow F_\beta \uparrow E_\xi \uparrow \mathcal{M} \downarrow$	$S_\alpha \uparrow F_\beta \uparrow E_\xi \uparrow \mathcal{M} \downarrow$	$S_\alpha \uparrow F_\beta \uparrow E_\xi \uparrow \mathcal{M} \downarrow$	$S_\alpha \uparrow F_\beta \uparrow E_\xi \uparrow \mathcal{M} \downarrow$	$S_\alpha \uparrow F_\beta \uparrow E_\xi \uparrow \mathcal{M} \downarrow$	$S_\alpha \uparrow F_\beta \uparrow E_\xi \uparrow \mathcal{M} \downarrow$	$S_\alpha \uparrow F_\beta \uparrow E_\xi \uparrow \mathcal{M} \downarrow$					
SSAL [5]	.803	.747	.865	.062	.863	.865	.908	.061	.785	.702	.835	.068	.865	.858	.923	.047	.798	.773	.854	.093	.750	.743	.801	.108
SSAL_T	.851	.793	.902	.048	.905	.894	.944	.040	.827	.745	.865	.063	.890	.868	.939	.040	.841	.822	.888	.073	.803	.784	.848	.090
SSAL_T_G	.847	.788	.896	.052	.908	.897	.945	.040	.825	.746	.861	.067	.896	.876	.942	.038	.839	.824	.886	.077	.819	.809	.869	.087
SSAL_T_S	.845	.799	.901	.051	.897	.892	.934	.047	.831	.763	.875	.056	.886	.874	.936	.042	.830	.815	.875	.082	.802	.790	.846	.096
Ours	<b>.867</b>	<b>.833</b>	<b>.926</b>	<b>.040</b>	<b>.910</b>	<b>.917</b>	<b>.952</b>	<b>.035</b>	<b>.842</b>	<b>.780</b>	<b>.888</b>	<b>.054</b>	<b>.906</b>	<b>.902</b>	<b>.956</b>	<b>.031</b>	<b>.853</b>	<b>.836</b>	<b>.903</b>	<b>.062</b>	<b>.821</b>	<b>.825</b>	<b>.877</b>	<b>.078</b>

TABLE 7  
Depth contribution analysis.

Method	DUTS [6]				ECSSD [78]				DUT [11]				HKU-IS [74]				PASCAL-S [79]				SOD [80]			
	$S_\alpha \uparrow F_\beta \uparrow E_\xi \uparrow \mathcal{M} \downarrow$	$S_\alpha \uparrow F_\beta \uparrow E_\xi \uparrow \mathcal{M} \downarrow$	$S_\alpha \uparrow F_\beta \uparrow E_\xi \uparrow \mathcal{M} \downarrow$	$S_\alpha \uparrow F_\beta \uparrow E_\xi \uparrow \mathcal{M} \downarrow$	$S_\alpha \uparrow F_\beta \uparrow E_\xi \uparrow \mathcal{M} \downarrow$	$S_\alpha \uparrow F_\beta \uparrow E_\xi \uparrow \mathcal{M} \downarrow$	$S_\alpha \uparrow F_\beta \uparrow E_\xi \uparrow \mathcal{M} \downarrow$	$S_\alpha \uparrow F_\beta \uparrow E_\xi \uparrow \mathcal{M} \downarrow$	$S_\alpha \uparrow F_\beta \uparrow E_\xi \uparrow \mathcal{M} \downarrow$	$S_\alpha \uparrow F_\beta \uparrow E_\xi \uparrow \mathcal{M} \downarrow$	$S_\alpha \uparrow F_\beta \uparrow E_\xi \uparrow \mathcal{M} \downarrow$	$S_\alpha \uparrow F_\beta \uparrow E_\xi \uparrow \mathcal{M} \downarrow$	$S_\alpha \uparrow F_\beta \uparrow E_\xi \uparrow \mathcal{M} \downarrow$	$S_\alpha \uparrow F_\beta \uparrow E_\xi \uparrow \mathcal{M} \downarrow$	$S_\alpha \uparrow F_\beta \uparrow E_\xi \uparrow \mathcal{M} \downarrow$	$S_\alpha \uparrow F_\beta \uparrow E_\xi \uparrow \mathcal{M} \downarrow$	$S_\alpha \uparrow F_\beta \uparrow E_\xi \uparrow \mathcal{M} \downarrow$	$S_\alpha \uparrow F_\beta \uparrow E_\xi \uparrow \mathcal{M} \downarrow$	$S_\alpha \uparrow F_\beta \uparrow E_\xi \uparrow \mathcal{M} \downarrow$					
Fusion Strategies																								
Early fusion	.908	.883	.942	.028	.931	.934	.956	.029	.864	.811	.899	.046	.929	.925	.963	.024	.868	.868	.911	.059	.845	.848	.878	.074
Cross-level fusion	.915	.901	.946	.026	.937	.945	.958	.028	.867	.818	.899	.043	.931	.935	.962	.024	.874	.877	.914	.055	.847	.851	.874	.069
Late fusion	.917	.895	.948	.025	.939	.941	.962	.025	.867	.814	.899	.046	.930	.928	.963	.023	.868	.865	.909	.058	.855	.857	.888	.061
Ours	<b>.910</b>	<b>.891</b>	<b>.946</b>	<b>.027</b>	<b>.940</b>	<b>.945</b>	<b>.967</b>	<b>.023</b>	<b>.870</b>	<b>.824</b>	<b>.905</b>	<b>.042</b>	<b>.929</b>	<b>.928</b>	<b>.965</b>	<b>.023</b>	<b>.870</b>	<b>.871</b>	<b>.914</b>	<b>.056</b>	<b>.852</b>	<b>.862</b>	<b>.892</b>	<b>.064</b>

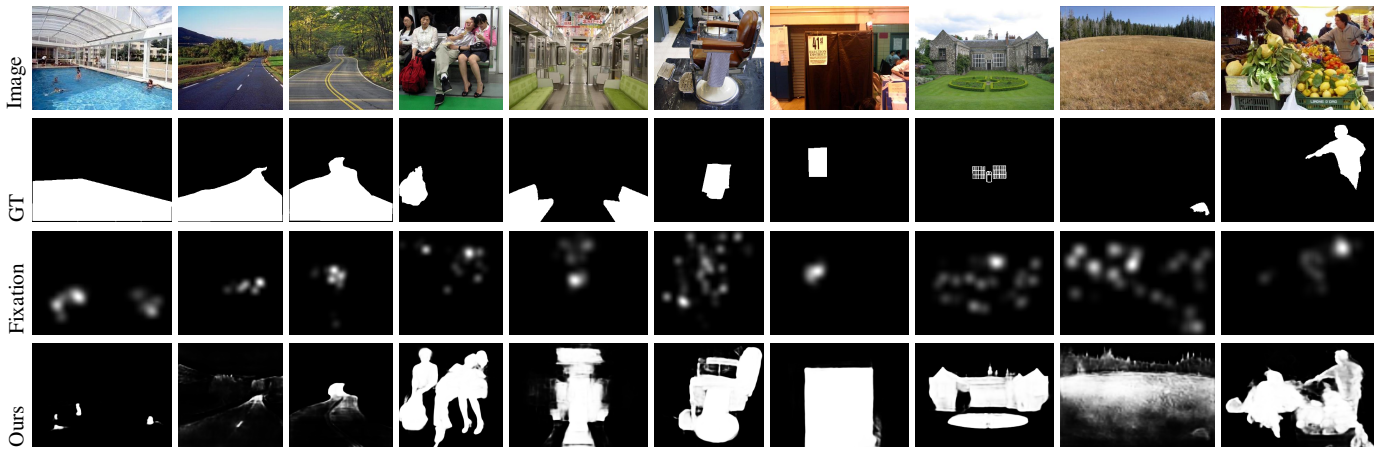


Fig. 15. Failure cases of our transformer backbone based RGB image salient object detection network on the DUT salient object testing dataset [11].

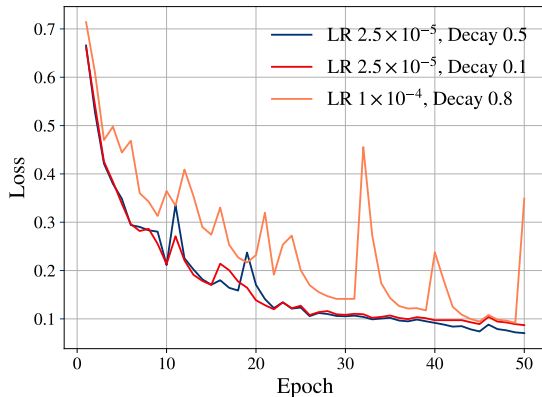


Fig. 16. Loss convergence curves of our transformer backbone based salient object detection network.

We then analysis how the extra depth information will help our salient object detection task. Firstly, we analyse different fusion strategies, and show model performance in Table 7 of the “Fusion

Strategies” section. Specifically, we design an early fusion model, cross-level fusion model and late fusion model to achieve RGB-D salient object detection with our DUTS training dataset [6], where the depth is computed with [22]. For the early fusion model, we adopt the same network as our RGB-D salient object detection model. For the cross-level fusion model, we feed RGB image and depth data to the transformer encoder to extract features of model modal. Then we concatenate the same stage of features of RGB branch and depth branch, and feed it to a  $3 \times 3$  convolutional layers to obtain feature map of same channel size as the RGB branch (or the depth branch). The same decoder is used to map the above feature to an one-channel saliency map. For the late fusion model, we obtain saliency from both RGB image as input, and depth data (we concatenate the one channel depth channel-wise to obtain a three-channel depth map) as input, and define our final prediction as the sum of saliency maps from both branches. Note that supervision is applied to all the three saliency predictions. Secondly, we analyse how different backbone networks impact on our pseudo depth based RGB-D salient object detection network, and show model performance in Table 7 of the “Different Backbones” section. Note

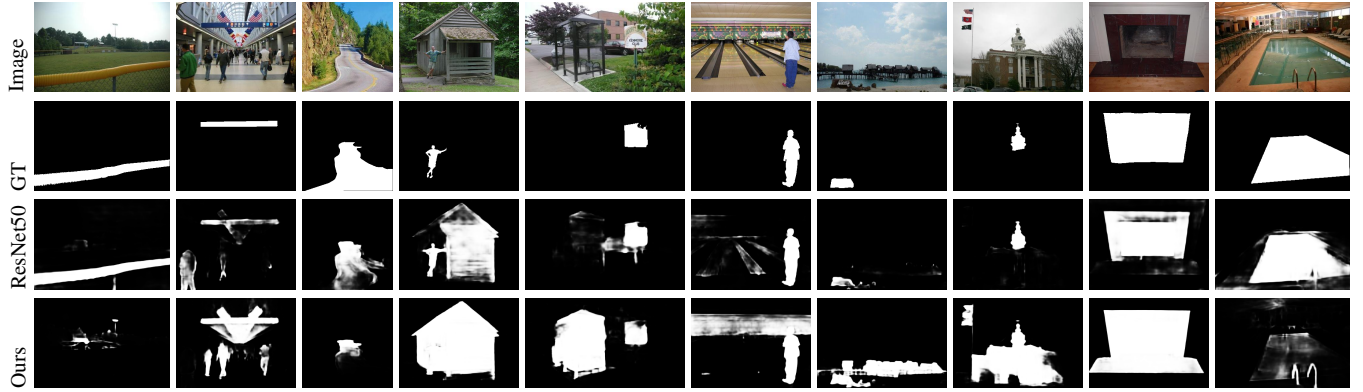


Fig. 17. Samples that ResNet50 [16] outperforms our transformer backbone based model.

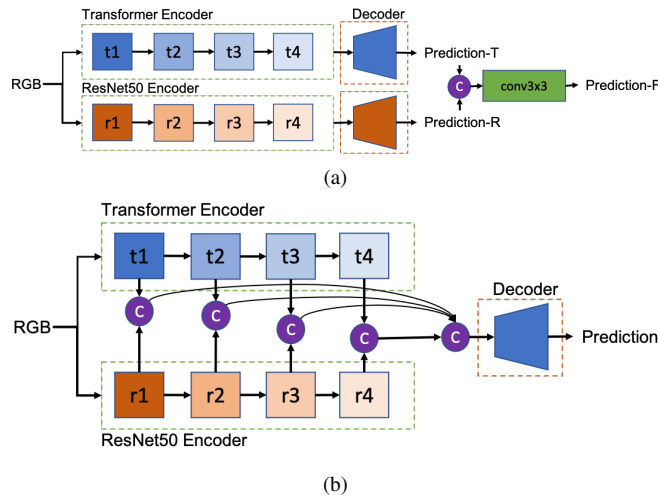


Fig. 18. The dual-backbone network with different fusion strategies: (a), Late fusion and (b): Cross-level fusion.

that, early fusion model is used for all the backbones. Model performance of the “Fusion Strategies” section compared with “Ours” (the RGB image based salient object detection model) in Table 7 indicates that the generated depth as shown in Fig. 13 may contains less complementary information as the RGB image, which leads to less contribution of pseudo depth for the RGB-D salient object detection model. Further, model performance in the “Different Backbones” compared with the “Early fusion” model in the “Fusion Strategies” section illustrates the effectiveness of transformer backbone for the RGB-D SOD model.

**Failure case analysis:** We analyse how our transformer backbone based model fails, and show some samples in Fig. 15, where the “Fixation” is the fixation map that show the fixation location of the salient objects. We notice that although our transformer model based prediction is incorrect compared with the provided ground truth map (“GT”) in Fig. 15, it is sometimes consistent with the fixation map. We can explain this phenomenon in two aspects. Firstly, the generated binary ground truth might be biased. Secondly, the global context modeling ability of transformer backbone may introduce extra noise to the model prediction, leading to false positive predictions. We also observe that the conventional backbone works better in some cases than the transformer backbone network, and show the samples in Fig. 17. With this observation,

we design two dual-backbone networks to combine the ResNet50 [16] backbone with the transformer backbone as shown in Fig. 18, where “t1, t2, t3 and t4” are different levels of feature for the transformer encoder, and “r1, r2, r3 and r4” are different levels of feature for the ResNet50 encoder. Note that, for the late fusion model, we have three predictions, and we define the prediction “Prediction-F” as our final prediction. For the cross-level fusion model, we only have one prediction in the end. The “Decoder” in Fig. 18 is the same as “Convolution Decoder” in Fig. 5. We also add the residual channel attention module [75] after each of the the encoder level fusion concatenation. We will work on the above two models to achieve adaptive context modeling by combining the conventional backbone, *e.g.*, ResNet50 [16] with the transformer backbone for salient object detection.

**Observations:** Due to the powerful encoder structure of transformer, the decoder of transformer can be designed very simply. We even noticed that the complex decoder module might not always lead to better performance, and it may decrease model performance if not well designed. Further, the transformer network is more sensitive to learning rate, and it is better to use a smaller learning rate for tasks with a small dataset.

## 5 CONCLUSION

In this paper, we have introduced the vision transformers for salient object detection and camouflaged object detection to exploit the global context information. Specifically, we design three fully supervised models for RGB salient object detection, RGB-D salient object detection and camouflaged object detection, which share the same network structure, except that we concatenate RGB image and depth data in the input layer and feed it to a  $3 \times 3$  convolutional layer to produce a three-channel feature map, which will be fed to the “Transformer Encoder” as shown in Fig. 5. Further, we introduce weakly supervised salient object detection network via scribble annotation by using the transformer backbone as shown in Fig. 7. Extensive experimental results in Section 4 proves the effectiveness of our transformer backbone based network, achieving new benchmark for RGB salient object detection, RGB-D salient object detection, camouflaged object detection and weakly supervised salient object detection. We also notice some failure cases as shown in Fig. 15, which indicates that the pure global context based transformer network may introduce noisy false positive to the model prediction. In the future, we plan to design an adaptive context modeling transformer network for effective salient/camouflage object detection.

## REFERENCES

[1] Z. Wu, L. Su, and Q. Huang, "Stacked cross refinement network for edge-aware salient object detection," in *Proceedings of the IEEE International Conference on Computer Vision (ICCV)*, pp. 7264–7273, 2019.

[2] J. Wei, S. Wang, and Q. Huang, "F<sup>3</sup>net: Fusion, feedback and focus for salient object detection," in *Proceedings of the AAAI Conference on Artificial Intelligence (AAAI)*, pp. 12321–12328, 2020.

[3] J. Zhang, D.-P. Fan, Y. Dai, S. Anwar, F. S. Saleh, T. Zhang, and N. Barnes, "UC-Net: Uncertainty inspired RGB-D saliency detection via conditional variational autoencoders," in *Proceedings of the IEEE Conference on Computer Vision and Pattern Recognition (CVPR)*, pp. 8582–8591, 2020.

[4] D.-P. Fan, Y. Zhai, A. Borji, J. Yang, and L. Shao, "BBS-Net: RGB-D salient object detection with a bifurcated backbone strategy network," in *Proceedings of the European Conference on Computer Vision (ECCV)*, pp. 275–292, 2020.

[5] J. Zhang, X. Yu, A. Li, P. Song, B. Liu, and Y. Dai, "Weakly-supervised salient object detection via scribble annotations," in *Proceedings of the IEEE Conference on Computer Vision and Pattern Recognition (CVPR)*, pp. 12546–12555, 2020.

[6] L. Wang, H. Lu, Y. Wang, M. Feng, D. Wang, B. Yin, and X. Ruan, "Learning to detect salient objects with image-level supervision," in *Proceedings of the IEEE Conference on Computer Vision and Pattern Recognition (CVPR)*, pp. 136–145, 2017.

[7] W. Wang, Q. Lai, H. Fu, J. Shen, H. Ling, and R. Yang, "Salient object detection in the deep learning era: An in-depth survey," *IEEE Transactions on Pattern Analysis and Machine Intelligence (T-PAMI)*, pp. 1–1, 2021.

[8] J. Zhang, T. Zhang, Y. Dai, M. Harandi, and R. Hartley, "Deep unsupervised saliency detection: A multiple noisy labeling perspective," in *Proceedings of the IEEE Conference on Computer Vision and Pattern Recognition (CVPR)*, pp. 9029–9038, 2018.

[9] D. T. Nguyen, M. Dax, C. K. Mummadgi, T. P. N. Ngo, T. H. P. Nguyen, Z. Lou, and T. Brox, "DeepUSPS: Deep robust unsupervised saliency prediction with self-supervision," in *Proceedings of the Advances in Neural Information Processing Systems (NeurIPS)*, 2019.

[10] W. Zhu, S. Liang, Y. Wei, and J. Sun, "Saliency optimization from robust background detection," in *Proceedings of the IEEE Conference on Computer Vision and Pattern Recognition (CVPR)*, pp. 2814–2821, 2014.

[11] C. Yang, L. Zhang, H. Lu, X. Ruan, and M.-H. Yang, "Saliency detection via graph-based manifold ranking," in *Proceedings of the IEEE Conference on Computer Vision and Pattern Recognition (CVPR)*, pp. 3166–3173, 2013.

[12] M.-M. Cheng, N. J. Mitra, X. Huang, P. H. Torr, and S.-M. Hu, "Global contrast based salient region detection," *IEEE Transactions on Pattern Analysis and Machine Intelligence (T-PAMI)*, vol. 37, no. 3, pp. 569–582, 2014.

[13] Z. Luo, A. Mishra, A. Achkar, J. Eichel, S. Li, and P.-M. Jodoin, "Non-local deep features for salient object detection," in *Proceedings of the IEEE Conference on Computer Vision and Pattern Recognition (CVPR)*, pp. 6609–6617, 2017.

[14] N. Liu, J. Han, and M.-H. Yang, "Picanet: Learning pixel-wise contextual attention for saliency detection," in *Proceedings of the IEEE Conference on Computer Vision and Pattern Recognition (CVPR)*, pp. 3089–3098, 2018.

[15] K. Simonyan and A. Zisserman, "Very deep convolutional networks for large-scale image recognition," in *Proceedings of the The International Conference on Learning Representations (ICLR)* (Y. Bengio and Y. LeCun, eds.), 2015.

[16] K. He, X. Zhang, S. Ren, and J. Sun, "Deep residual learning for image recognition," in *Proceedings of the IEEE Conference on Computer Vision and Pattern Recognition (CVPR)*, pp. 770–778, 2016.

[17] Z. Wu, L. Su, and Q. Huang, "Cascaded partial decoder for fast and accurate salient object detection," in *Proceedings of the IEEE Conference on Computer Vision and Pattern Recognition (CVPR)*, pp. 3907–3916, 2019.

[18] L. Itti, C. Koch, and E. Niebur, "A model of saliency-based visual attention for rapid scene analysis," *IEEE Transactions on Pattern Analysis and Machine Intelligence (T-PAMI)*, vol. 20, no. 11, pp. 1254–1259, 1998.

[19] R. Achanta, S. Hemami, F. Estrada, and S. Sussstrunk, "Frequency-tuned salient region detection," in *Proceedings of the IEEE Conference on Computer Vision and Pattern Recognition (CVPR)*, pp. 1597–1604, 2009.

[20] G. Li and Y. Yu, "Visual saliency based on multiscale deep features," in *Proceedings of the IEEE Conference on Computer Vision and Pattern Recognition (CVPR)*, 2015.

[21] A. Vaswani, N. Shazeer, N. Parmar, J. Uszkoreit, L. Jones, A. N. Gomez, L. Kaiser, and I. Polosukhin, "Attention is all you need," in *Proceedings of the Advances in Neural Information Processing Systems (NeurIPS)*, 2017.

[22] R. Ranftl, A. Bochkovskiy, and V. Koltun, "Vision transformers for dense prediction," *arXiv preprint arXiv:2103.13413*, 2021.

[23] A. Obukhov, S. Georgoulis, D. Dai, and L. Van Gool, "Gated CRF loss for weakly supervised semantic image segmentation," in *Proceedings of the Advances in Neural Information Processing Systems (NeurIPS)*, 2019.

[24] B. Wang, Q. Chen, M. Zhou, Z. Zhang, X. Jin, and K. Gai, "Progressive feature polishing network for salient object detection," in *Proceedings of the AAAI Conference on Artificial Intelligence (AAAI)*, pp. 12128–12135, 2020.

[25] X. Qin, Z. Zhang, C. Huang, C. Gao, M. Dehghan, and M. Jagersand, "Basnet: Boundary-aware salient object detection," in *Proceedings of the IEEE Conference on Computer Vision and Pattern Recognition (CVPR)*, pp. 7479–7489, 2019.

[26] Y. Pang, X. Zhao, L. Zhang, and H. Lu, "Multi-scale interactive network for salient object detection," in *Proceedings of the IEEE Conference on Computer Vision and Pattern Recognition (CVPR)*, pp. 9413–9422, 2020.

[27] G. Li, Y. Xie, and L. Lin, "Weakly supervised salient object detection using image labels," in *Proceedings of the AAAI Conference on Artificial Intelligence (AAAI)*, 2018.

[28] S. Yu, B. Zhang, J. Xiao, and E. G. Lim, "Structure-consistent weakly supervised salient object detection with local saliency coherence," in *Proceedings of the AAAI Conference on Artificial Intelligence (AAAI)*, 2021.

[29] X. Li, F. Yang, H. Cheng, W. Liu, and D. Shen, "Contour knowledge transfer for salient object detection," in *Proceedings of the European Conference on Computer Vision (ECCV)*, pp. 355–370, 2018.

[30] D. Zhang, J. Han, and Y. Zhang, "Supervision by fusion: Towards unsupervised learning of deep salient object detector," in *Proceedings of the IEEE International Conference on Computer Vision (ICCV)*, pp. 4048–4056, 2017.

[31] L. Qu, S. He, J. Zhang, J. Tian, Y. Tang, and Q. Yang, "RGBD salient object detection via deep fusion," *IEEE Transactions on Image Processing (TIP)*, vol. 26, no. 5, pp. 2274–2285, 2017.

[32] N. Wang and X. Gong, "Adaptive fusion for RGB-D salient object detection," *IEEE Access*, vol. 7, pp. 55277–55284, 2019.

[33] J. Han, H. Chen, N. Liu, C. Yan, and X. Li, "CNNs-based RGB-D saliency detection via cross-view transfer and multiview fusion," *IEEE transactions on cybernetics*, vol. 48, no. 11, pp. 3171–3183, 2017.

[34] Y. Piao, Z. Rong, M. Zhang, W. Ren, and H. Lu, "A2dele: Adaptive and attentive depth distiller for efficient RGB-D salient object detection," in *Proceedings of the IEEE Conference on Computer Vision and Pattern Recognition (CVPR)*, pp. 9060–9069, 2020.

[35] Y. Piao, W. Ji, J. Li, M. Zhang, and H. Lu, "Depth-induced multi-scale recurrent attention network for saliency detection," in *Proceedings of the IEEE International Conference on Computer Vision (ICCV)*, pp. 7254–7263, 2019.

[36] H. Chen and Y. Li, "Progressively complementarity-aware fusion network for RGB-D salient object detection," in *Proceedings of the IEEE Conference on Computer Vision and Pattern Recognition (CVPR)*, pp. 3907–3916, 2019.

the IEEE Conference on Computer Vision and Pattern Recognition (CVPR), pp. 3051–3060, 2018.

[37] H. Chen, Y. Li, and D. Su, “Multi-modal fusion network with multi-scale multi-path and cross-modal interactions for RGB-D salient object detection,” *Pattern Recognition (PR)*, vol. 86, pp. 376–385, 2019.

[38] H. Chen and Y. Li, “Three-stream attention-aware network for RGB-D salient object detection,” *IEEE Transactions on Image Processing (TIP)*, vol. 28, no. 6, pp. 2825–2835, 2019.

[39] J.-X. Zhao, Y. Cao, D.-P. Fan, M.-M. Cheng, X.-Y. Li, and L. Zhang, “Contrast prior and fluid pyramid integration for RGBD salient object detection,” in *Proceedings of the IEEE Conference on Computer Vision and Pattern Recognition (CVPR)*, pp. 3927–3936, 2019.

[40] M. Zhang, W. Ren, Y. Piao, Z. Rong, and H. Lu, “Select, supplement and focus for RGB-D saliency detection,” in *Proceedings of the IEEE Conference on Computer Vision and Pattern Recognition (CVPR)*, pp. 3472–3481, 2020.

[41] N. Liu, N. Zhang, and J. Han, “Learning selective self-mutual attention for RGB-D saliency detection,” in *Proceedings of the IEEE Conference on Computer Vision and Pattern Recognition (CVPR)*, pp. 13756–13765, 2020.

[42] W. Ji, J. Li, M. Zhang, Y. Piao, and H. Lu, “Accurate RGB-D salient object detection via collaborative learning,” in *Proceedings of the European Conference on Computer Vision (ECCV)*, 2020.

[43] Y. Pang, L. Zhang, X. Zhao, and H. Lu, “Hierarchical dynamic filtering network for RGB-D salient object detection,” in *Proceedings of the European Conference on Computer Vision (ECCV)*, 2020.

[44] Z. Zhang, Z. Lin, J. Xu, W.-D. Jin, S.-P. Lu, and D.-P. Fan, “Bilateral attention network for RGB-D salient object detection,” *IEEE Transactions on Image Processing (TIP)*, vol. 30, pp. 1949–1961, 2021.

[45] C. Li, R. Cong, Y. Piao, Q. Xu, and C. C. Loy, “RGB-D salient object detection with cross-modality modulation and selection,” in *Proceedings of the European Conference on Computer Vision (ECCV)*, pp. 225–241, 2020.

[46] G. Li, Z. Liu, L. Ye, Y. Wang, and H. Ling, “Cross-modal weighting network for RGB-D salient object detection,” in *Proceedings of the European Conference on Computer Vision (ECCV)*, pp. 665–681, 2020.

[47] A. Luo, X. Li, F. Yang, Z. Jiao, H. Cheng, and S. Lyu, “Cascade graph neural networks for RGB-D salient object detection,” in *Proceedings of the European Conference on Computer Vision (ECCV)*, pp. 346–364, 2020.

[48] S. Chen and Y. Fu, “Progressively guided alternate refinement network for RGB-D salient object detection,” in *Proceedings of the European Conference on Computer Vision (ECCV)*, pp. 520–538, 2020.

[49] M. Zhang, S. X. Fei, J. Liu, S. Xu, Y. Piao, and H. Lu, “Asymmetric two-stream architecture for accurate RGB-D saliency detection,” in *Proceedings of the European Conference on Computer Vision (ECCV)*, pp. 374–390, 2020.

[50] S. Merilaita, N. E. Scott-Samuel, and I. C. Cuthill, “How camouflage works,” *Philosophical Transactions of the Royal Society B: Biological Sciences*, vol. 372, no. 1724, p. 20160341, 2017.

[51] J. Troscianko, J. Skelhorn, and M. Stevens, “Quantifying camouflage: how to predict detectability from appearance,” *BMC evolutionary biology*, vol. 17, no. 1, pp. 1–13, 2017.

[52] T. W. Pike, “Quantifying camouflage and conspicuousness using visual salience,” *Methods in Ecology and Evolution*, vol. 9, no. 8, pp. 1883–1895, 2018.

[53] A. Tankus and Y. Yeshurun, “Convexity-based visual camouflage breaking,” *Computer Vision and Image Understanding*, vol. 82, no. 3, pp. 208–237, 2001.

[54] F. Xue, C. Yong, S. Xu, H. Dong, Y. Luo, and W. Jia, “Camouflage performance analysis and evaluation framework based on features fusion,” *Multimedia Tools and Applications*, vol. 75, no. 7, pp. 4065–4082, 2016.

[55] S. Li, D. Florencio, Y. Zhao, C. Cook, and W. Li, “Foreground detection in camouflaged scenes,” in *Proceedings of the IEEE International Conference on Image Processing (ICIP)*, pp. 4247–4251, IEEE, 2017.

[56] T.-N. Le, T. V. Nguyen, Z. Nie, M.-T. Tran, and A. Sugimoto, “Anabranch network for camouflaged object segmentation,” *Computer Vision and Image Understanding*, vol. 184, pp. 45–56, 2019.

[57] D.-P. Fan, G.-P. Ji, G. Sun, M.-M. Cheng, J. Shen, and L. Shao, “Camouflaged object detection,” in *Proceedings of the IEEE Conference on Computer Vision and Pattern Recognition (CVPR)*, pp. 2777–2787, 2020.

[58] J. Ren, X. Hu, L. Zhu, X. Xu, Y. Xu, W. Wang, Z. Deng, and P.-A. Heng, “Deep texture-aware features for camouflaged object detection,” *arXiv preprint arXiv:2102.02996*, 2021.

[59] B. Dong, M. Zhuge, Y. Wang, H. Bi, and G. Chen, “Towards accurate camouflaged object detection with mixture convolution and interactive fusion,” *arXiv preprint arXiv:2101.05687*, 2021.

[60] N. Carion, F. Massa, G. Synnaeve, N. Usunier, A. Kirillov, and S. Zagoruyko, “End-to-end object detection with transformers,” in *Proceedings of the European Conference on Computer Vision (ECCV)*, pp. 213–229, 2020.

[61] X. Zhu, W. Su, L. Lu, B. Li, X. Wang, and J. Dai, “Deformable DETR: Deformable transformers for end-to-end object detection,” in *Proceedings of the The International Conference on Learning Representations (ICLR)*, 2021.

[62] Z. Dai, B. Cai, Y. Lin, and J. Chen, “UP-DETR: Unsupervised pre-training for object detection with transformers,” *Proceedings of the IEEE Conference on Computer Vision and Pattern Recognition (CVPR)*, 2021.

[63] W. Wang, E. Xie, X. Li, D.-P. Fan, K. Song, D. Liang, T. Lu, P. Luo, and L. Shao, “Pyramid vision transformer: A versatile backbone for dense prediction without convolutions,” *arXiv preprint arXiv:2102.12122*, 2021.

[64] G. Zhang, Z. Luo, K. Cui, and S. Lu, “Meta-DETR: Few-shot object detection via unified image-level meta-learning,” *arXiv preprint arXiv:2103.11731*, 2021.

[65] S. Zheng, J. Lu, H. Zhao, X. Zhu, Z. Luo, Y. Wang, Y. Fu, J. Feng, T. Xiang, P. H. Torr, and L. Zhang, “Rethinking semantic segmentation from a sequence-to-sequence perspective with transformers,” *Proceedings of the IEEE Conference on Computer Vision and Pattern Recognition (CVPR)*, 2021.

[66] Y. Xu, Y. Ban, G. Delorme, C. Gan, D. Rus, and X. Alameda-Pineda, “TransCenter: Transformers with dense queries for multiple-object tracking,” *arXiv preprint arXiv:2103.15145*, 2021.

[67] P. Chu, J. Wang, Q. You, H. Ling, and Z. Liu, “Spatial-temporal graph transformer for multiple object tracking,” *arXiv preprint arXiv:2104.00194*, 2021.

[68] B. Yan, H. Peng, J. Fu, D. Wang, and H. Lu, “Learning spatio-temporal transformer for visual tracking,” *arXiv preprint arXiv:2103.17154*, 2021.

[69] W. Mao, Y. Ge, C. Shen, Z. Tian, X. Wang, and Z. Wang, “TFPose: Direct human pose estimation with transformers,” *arXiv preprint arXiv:2103.15320*, 2021.

[70] L. Stoffl, M. Vidal, and A. Mathis, “End-to-End trainable Multi-Instance pose estimation with transformers,” *arXiv preprint arXiv:2103.12115*, 2021.

[71] S. Jiang, D. Campbell, Y. Lu, H. Li, and R. Hartley, “Learning to estimate hidden motions with global motion aggregation,” *arXiv preprint arXiv:2104.02409*, 2021.

[72] A. Dosovitskiy, L. Beyer, A. Kolesnikov, D. Weissenborn, X. Zhai, T. Unterthiner, M. Dehghani, M. Minderer, G. Heigold, S. Gelly, J. Uszkoreit, and N. Houlsby, “An image is worth 16x16 words: Transformers for image recognition at scale,” in *Proceedings of the The International Conference on Learning Representations (ICLR)*, 2021.

[73] K. Han, Y. Wang, H. Chen, X. Chen, J. Guo, Z. Liu, Y. Tang, A. Xiao, C. Xu, Y. Xu, et al., “A survey on visual transformer,”

*arXiv preprint arXiv:2012.12556*, 2020.

[74] G. Li and Y. Yu, “Visual saliency based on multiscale deep features,” in *Proceedings of the IEEE Conference on Computer Vision and Pattern Recognition (CVPR)*, pp. 5455–5463, 2015.

[75] Y. Zhang, K. Li, K. Li, L. Wang, B. Zhong, and Y. Fu, “Image super-resolution using very deep residual channel attention networks,” in *Proceedings of the European Conference on Computer Vision (ECCV)*, pp. 286–301, 2018.

[76] Y. Wang, Y. Yang, Z. Yang, L. Zhao, P. Wang, and W. Xu, “Occlusion aware unsupervised learning of optical flow,” in *Proceedings of the IEEE Conference on Computer Vision and Pattern Recognition (CVPR)*, pp. 4884–4893, 2018.

[77] H. Zhou, X. Xie, J.-H. Lai, Z. Chen, and L. Yang, “Interactive two-stream decoder for accurate and fast saliency detection,” in *Proceedings of the IEEE Conference on Computer Vision and Pattern Recognition (CVPR)*, pp. 9141–9150, 2020.

[78] Q. Yan, L. Xu, J. Shi, and J. Jia, “Hierarchical saliency detection,” in *Proceedings of the IEEE Conference on Computer Vision and Pattern Recognition (CVPR)*, pp. 1155–1162, 2013.

[79] Y. Li, X. Hou, C. Koch, J. M. Rehg, and A. L. Yuille, “The secrets of salient object segmentation,” in *Proceedings of the IEEE Conference on Computer Vision and Pattern Recognition (CVPR)*, pp. 280–287, 2014.

[80] V. Movahedi and J. H. Elder, “Design and perceptual validation of performance measures for salient object segmentation,” in *Proceedings of the IEEE Conference on Computer Vision and Pattern Recognition Workshops (CVPRW)*, pp. 49–56, 2010.

[81] J.-J. Liu, Q. Hou, M.-M. Cheng, J. Feng, and J. Jiang, “A simple pooling-based design for real-time salient object detection,” in *Proceedings of the IEEE Conference on Computer Vision and Pattern Recognition (CVPR)*, pp. 3917–3926, 2019.

[82] J.-X. Zhao, J.-J. Liu, D.-P. Fan, Y. Cao, J. Yang, and M.-M. Cheng, “EGNet:edge guidance network for salient object detection,” in *Proceedings of the IEEE International Conference on Computer Vision (ICCV)*, pp. 8779–8788, 2019.

[83] P. Skurowski, H. Abdulameer, J. Błaszczyk, T. Depta, A. Kornacki, and P. Koziel, “Animal camouflage analysis: Chameleon database,” in *Unpublished Manuscript*, 2018.

[84] Y. Lv, J. Zhang, Y. Dai, A. Li, B. Liu, N. Barnes, and D.-P. Fan, “Simultaneously localize, segment and rank the camouflaged objects,” in *Proceedings of the IEEE Conference on Computer Vision and Pattern Recognition (CVPR)*, 2021.

[85] R. Ju, Y. Liu, T. Ren, L. Ge, and G. Wu, “Depth-aware salient object detection using anisotropic center-surround difference,” *Signal Processing: Image Communication*, vol. 38, pp. 115 – 126, 2015.

[86] H. Peng, B. Li, W. Xiong, W. Hu, and R. Ji, “RGBD salient object detection: A benchmark and algorithms,” in *Proceedings of the European Conference on Computer Vision (ECCV)*, pp. 92–109, 2014.

[87] N. Li, J. Ye, Y. Ji, H. Ling, and J. Yu, “Saliency detection on light field,” in *Proceedings of the IEEE Conference on Computer Vision and Pattern Recognition (CVPR)*, pp. 2806–2813, 2014.

[88] Y. Cheng, H. Fu, X. Wei, J. Xiao, and X. Cao, “Depth enhanced saliency detection method,” in *Proceedings of international conference on internet multimedia computing and service*, pp. 23–27, 2014.

[89] Y. Niu, Y. Geng, X. Li, and F. Liu, “Leveraging stereopsis for saliency analysis,” in *Proceedings of the IEEE Conference on Computer Vision and Pattern Recognition (CVPR)*, pp. 454–461, 2012.

[90] D.-P. Fan, Z. Lin, Z. Zhang, M. Zhu, and M.-M. Cheng, “Rethinking RGB-D Salient Object Detection: Models, Datasets, and Large-Scale Benchmarks,” *IEEE Transactions on neural networks and learning systems*, 2020.

[91] D.-P. Fan, C. Gong, Y. Cao, B. Ren, M.-M. Cheng, and A. Borji, “Enhanced-alignment measure for binary foreground map evaluation,” *Proceedings of the International Joint Conferences on Artificial Intelligence (IJCAI)*, pp. 698–704, 2018.

[92] D.-P. Fan, M.-M. Cheng, Y. Liu, T. Li, and A. Borji, “Structure-measure: A new way to evaluate foreground maps,” in *Proceedings of the IEEE International Conference on Computer Vision (ICCV)*, pp. 4548–4557, 2017.

[93] S.-H. Gao, Y.-Q. Tan, M.-M. Cheng, C. Lu, Y. Chen, and S. Yan, “Highly efficient salient object detection with 100k parameters,” in *Proceedings of the European Conference on Computer Vision (ECCV)*, pp. 702–721, 2020.

[94] A. Li, J. Zhang, Y. Lv, B. Liu, T. Zhang, and Y. Dai, “Uncertainty-aware joint salient object and camouflaged object detection,” in *Proceedings of the IEEE Conference on Computer Vision and Pattern Recognition (CVPR)*, 2021.

[95] K. Fu, D.-P. Fan, G.-P. Ji, and Q. Zhao, “JL-DCF: Joint learning and densely-cooperative fusion framework for RGB-D salient object detection,” in *Proceedings of the IEEE Conference on Computer Vision and Pattern Recognition (CVPR)*, pp. 3052–3062, 2020.